Research Paper

Radionuclide-based molecular imaging allows CAR-T cellular visualization and therapeutic monitoring

Fuqiang Shao[1,2,3,4], Yu Long[1,2], Hao Ji[1,2], Dawei Jiang[1,2], Ping Lei[5], Xiaoli Lan[1,2✉]

1. Department of Nuclear Medicine, Union Hospital, Tongji Medical College, Huazhong University of Science and Technology, Wuhan 430022, China.
2. Hubei Key Laboratory of Molecular Imaging, Wuhan 430022, China.
3. Department of nuclear medicine, Zigong First People's Hospital, Zigong 643000, China.
4. Nuclear Medicine and Molecular Imaging Key Laboratory of Sichuan Province, Luzhou 646000, China.
5. Department of Immunology, School of Basic Medicine, Tongji Medical College, Huazhong University of Science and Technology, Wuhan 430030, China.

✉ Corresponding author: Xiaoli Lan, MD, Ph.D. Department of Nuclear Medicine, Union Hospital, Tongji Medical College, Huazhong University of Science and Technology, No. 1277 Jiefang Ave, Wuhan, 430022, China. Tel.: +86-27-83692633 (O), +86-13886193262 (mobile); E-mail: xiaoli_lan@hust.edu.cn.

Abstract

Chimeric antigen receptor T cell (CAR-T) therapy is a new and effective form of adoptive cell therapy that is rapidly entering the mainstream for the treatment of CD19-positive hematological cancers because of its impressive effect and durable responses. Huge challenges remain in achieving similar success in patients with solid tumors. The current methods of monitoring CAR-T, including morphological imaging (CT and MRI), blood tests, and biopsy, have limitations to assess whether CAR-T cells are homing to tumor sites and infiltrating into tumor bed, or to assess the survival, proliferation, and persistence of CAR-T cells in solid tumors associated with an immunosuppressive microenvironment. Radionuclide-based molecular imaging affords improved CAR-T cellular visualization and therapeutic monitoring through either a direct cellular radiolabeling approach or a reporter gene imaging strategy, and endogenous cell imaging is beneficial to reflect functional information and immune status of T cells. Focusing on the dynamic monitoring and precise assessment of CAR-T therapy, this review summarizes the current applications of radionuclide-based noninvasive imaging in CAR-T cells visualization and monitoring and presents current challenges and strategic choices.

Key words: chimeric antigen receptor T cell; molecular imaging; side effects; therapeutic monitoring; direct labeling; reporter gene; endogenous cell

Introduction

Immunotherapy is becoming the mainstay of cancer treatment after conventional approaches (surgery, radiotherapy, and chemotherapy) have failed. Immunotherapeutic strategies include vaccines, immune checkpoint blockade, antibody-drug conjugates, radionuclide-labeled antibodies, and, most recently, adoptive cell therapies (ACT) [1]. The development of ACT has mainly focused on the construction of a chimeric antigen receptor (CAR)-T cell [2, 3]. CAR-T cells' antitumor activity is the result of the formation of an immune synapse with target cells, leading to expression of pro-apoptotic ligands and accompanied by the release of cytotoxic perforin and granzyme and the secretion of pro-inflammatory cytokines (such as interferon [IFN]-α, IFN-γ, and interleukin 2 [IL-2]) by the T cells. This results in the activation of endogenous immune responses [3]. CD19-targeting T cells, the most representative form of CAR-T therapy, uses autologous T cells engineered to express the CD19 antigen receptor. They attack CD19-positive malignancies with high affinity, and produce durable response [4, 5], resulting in better curative effect in patients with leukemia or lymphoma [6-8].

However, several clinical trials have shown that CAR-T therapy in solid tumors remains unsatisfactory. The main reasons may be related to the difficulties of defining tumor specific targets, the limited CAR-T cells trafficking to the tumor site, and the immunosuppressive microenvironment of solid

tumors [2, 9-13]. Several strategies are being dedicated to serve these problems [2, 13-17]. Providing that these obstacles can be overcome, CAR-T therapy may have great potential to treat solid tumors.

Because CAR-T cells are a "living drug" and their migration, localization, infiltration, expansion, and persistence of CAR-T cells after infusion are dynamic processes [17]. The safety of CAR-T cell therapy has always been a concern, as it is frequently accompanied by severe adverse effects, such as on-target off-tumor toxicity, neurotoxicity, and cytokine release syndrome. These are still the chief impediments to CAR-T therapy [18, 19]. Dynamic monitoring of CAR-T cells would improve the understanding of cellular *in vivo* behaviour, which may allow optimization of the infusion timing and dose [20]. It may also help avoid potential lethal systemic toxicity. Therefore, many questions pose great challenges for CAR-T monitoring. For example, can the transferred cells home to the tumor site? Can the cells infiltrate the tumor bed? How many cells infiltrate into the tumor? How long can the cells retention in the tumor? When did the expansion and contraction happen? Are the cells off-target to settle in extratumor tissues? Can the cells infiltrated in the tumor site play a tumor killing effect?

Current monitoring in CAR-T cell studies has mainly focused on disease response assessment, on CAR-T cell persistence, expansion, and effector function, and on serum cytokine (such as IFN-α, IFN-γ and IL-2) and immune marker levels [17]. In solid tumors, the disease response assessment usually depends on the tumor size and morphological change detection by computed tomography (CT) and/or magnetic resonance imaging (MRI), which can provide information about the tumor burden, but the spatial information of infused T cells is undetectable [21, 22]. Similarly, although peripheral blood tests can assay adoptively transferred T cells and associated cytokines or immune markers in the circulation, they are unable to show the spatial distribution and tumor-specific expansion of infused T cells, and the blood values measured may not accurately quantify the extent of tumor infiltration [17].

Surveillance of adoptively transferred CAR-T cells can also be achieved through tumor tissue biopsy, but the information obtained strongly depends on sampling, which often only involves a small part of the tumor tissue and cannot fully reflect T cells infiltration in entire tumor [21]. The development of visualization tools that go beyond anatomical imaging and provide spatial information of cells, is key to achieving dynamic, non-invasive monitoring of therapeutic cells.

Molecular imaging is a novel and rapidly developing discipline combining molecular biology and medical imaging techniques to allow the visualization of biological processes [23-25]. Different molecular imaging modalities have their own advantages and disadvantages. Optical imaging (OI), such as bioluminescence imaging (BLI) and fluorescence imaging (FLI), can offer great sensitivity at a lower cost and higher throughput [26]. OI is suitable for *in vitro* studies and frequent small animal imaging [27], but several shortcomings block the clinical translation, such as lack of tomographic information, inability to image deep tissue, poor spatial resolution, and mass quantity (g to mg) of probe needed [26, 28, 29]. Although MRI has a high spatial resolution and excellent soft tissue contrast, without ionizing radiation [30, 31], it is handicapped by the inherently relatively lower sensitivity in comparison to OI and nuclear imaging [32]. Radionuclide-based imaging, including positron-emission tomography (PET) and single-photon emission computed tomography (SPECT) paired with CT (PET/CT, SPECT/CT) or MRI (PET/MRI) afford high sensitivity, multiple available probes, and a combination of quantitative physiological and tomographic information [33, 34]. Despite the shortcomings such as radiation exposure, expense, and low spatial resolution, PET/SPECT imaging techniques remain the greatest clinical translation potential compared with OI and MRI [35-37].

So far, radionuclide-based T cells imaging techniques include two main categories, direct labeling approach, or the reporter gene strategy [35, 38]. The former refers to the T cells are passively labeled with radionuclides or radioactive materials *in vitro* [39, 40], and the latter depends on the expression of an enzyme, receptor, or transporter by reporter gene-transduced T cells [41-45]. Several studies in animal models, as well as clinical trials, have demonstrated that radionuclide-based imaging allow directly (*ex vivo* labeling) or indirectly (reporter gene) visualization of CAR-T cells *in vivo*, which would provide crucial information about the proportion of viable cells and their biodistribution (**Figure 1**). In addition, endogenous T cell imaging can reflect the cellular activation and functional status by targeting cell surface markers or key materials in the metabolic pathways [35, 46, 47], which could be applied as a supplementary strategy for the two main imaging techniques.

This review aims to provide an overview of the most recent developments in PET/SPECT imaging based on direct labeling and reporter gene strategy for the visualizing and monitoring of CAR-T cells, as well as the current applications of endogenous T cell imaging in the cellular field. The advantages and

disadvantages of these imaging strategies were discussed and the key aspects of imaging strategy choice are summarized for looking forward the future progress.

Direct labeling approach

As shown in **Figure 1**, T-cells derived from patients or healthy donors are transduced with a CAR-encoding gene to generate CAR-T cells. After expansion and characterization, the CAR-T cells could be *in vitro* labeled with radionuclide for imaging. The major advantage of direct labeling approach is the simple nature of the labeling process, which requires minimal manipulation of the cells. Recent publications [48-50] have shown that CAR-T cells can be radiolabeled directly using a range of materials such as small molecules and nanoparticles.

Small molecule-based labeling

Two CAR-T cells, targeting transmembrane glycoprotein Mucin 1 (MUC1) and the extended ErbB network respectively, were developed by Parente-Pereira et al. CAR-T cells were passively labeled with ^{111}In-tropolonate to allow high-resolution real-time cellular tracking by SPECT/CT imaging [48]. When they were infused intravenously into tumor-bearing severe combined immunodeficiency

(SCID) Beige mice (MUC1-targeting CAR-T for MDA-MB-435 breast cancer, and ErbB-targeting CAR-T for HN3 human head and neck squamous cell carcinoma), the engineered CAR-T cells distributed in the murine lungs, liver, and spleen without significant penetration into the tumor. When infused via either the intraperitoneal or subcutaneous route, the CAR-T cells remained mostly at the site of injection. This provided first-hand experience of direct cellular radiolabeling in CAR-T therapy and enabled successful tracking of cell migration *in vivo*.

Another small molecule, oxine, has been often used in the labeling and tracing of murine lymphocytes [51-53]. Weist et al. [49] first used oxine for the radiolabeling of human-derived CAR-T cells. They engineered two different CAR-T cell lines (interleukin-13 receptor α2 [IL13Rα2]-CAR-T and prostate stem cell antigen [PSCA]-CAR-T) and labeled them with [89]Zr-oxine. [89]Zr-oxine-CAR-T cells maintained *in vivo* cytokine production, migration, tumor cytotoxicity, and *in vitro* anti-tumor activity at a labeling density of 70 kBq per million cells. The radiolabeled IL13Rα2-CAR-T and PSCA-CAR-T cells were administered to glioblastoma- and prostate cancer-bearing nonobese diabetic severe combined immunodeficient (NSG) mice, respectively, and they were visualized by PET/CT imaging with relatively
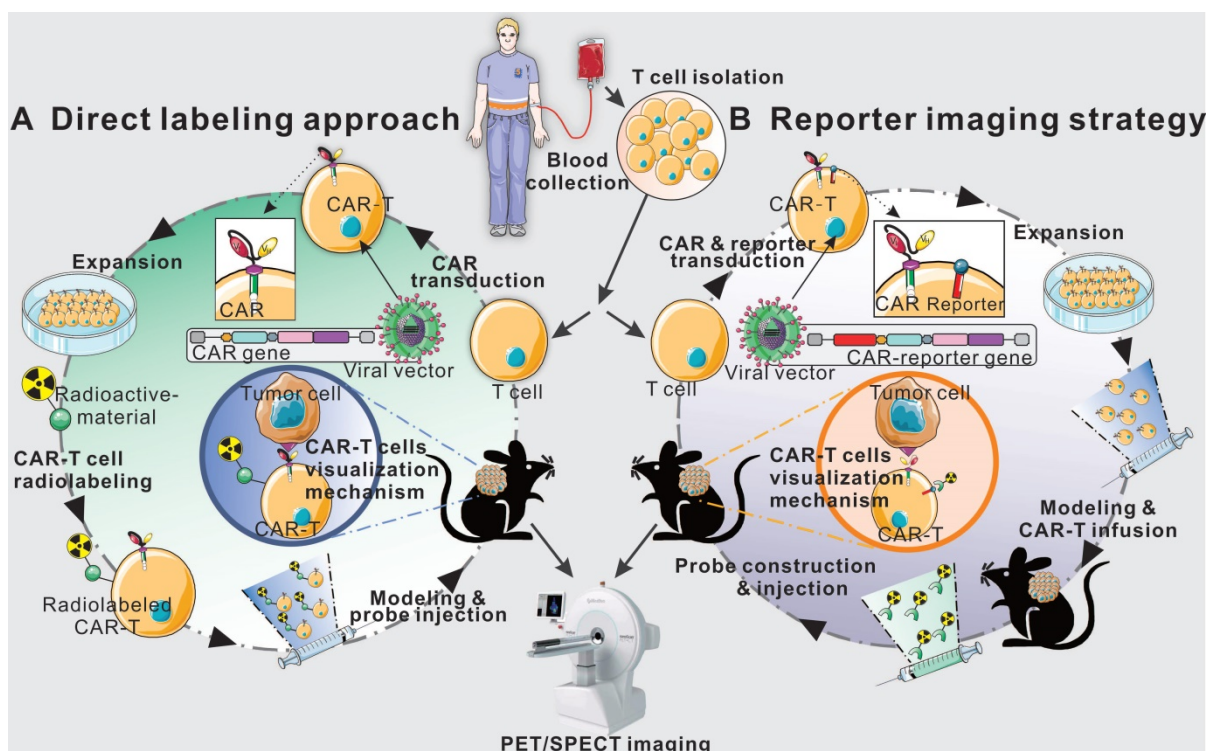

Figure 1. Schematic diagram of direct labeling approach and reporter gene imaging strategy. Blood is collected from patients or healthy donors, and peripheral blood mononuclear cells are isolated. Then, T cells are separated and harvested for further direct labeling or genetic modification. In the direct labeling approach (**A**), T cells are first transduced with a CAR-encoding gene to generate CAR-T cells. After expansion, CAR-T cells are radiolabeled with radioactive material, and then are infused into tumor-bearing mice. The radiolabeled CAR-T cells can be monitored by longitudinal PET/SPECT imaging. In the reporter imaging strategy (**B**), a recombinant gene for co-expressing CAR and reporter is transduced into T cells to generate reporter-CAR-T cells. After expansion, the reporter CAR-T cells are infused to tumor-bearing mice for treatment and longitudinal PET/SPECT monitoring.

high specificity (**Figure 2**). Additionally, since ^{89}Zr has a long physical half-life (78.4 h), the infused CAR-T cells could be traced and monitored dynamically on PET for up to 6 d. We cannot directly compare the two abovementioned studies because the nuclides, linkers, animal models, and modalities are different. However, Zr-89 is suitable for PET, which outperforms SPECT due to higher resolution and quantitative nature. Furthermore, compared to In-111, Zr-89 labeled cells can implement relatively longer imaging time window (96 h versus 6 d). Therefore, we believe the imaging performance of Zr-89 labeled CAR-T seems to be slightly better.

Nanomaterial-based labeling

Gold nanoparticles (GNPs) have been found appropriate for intracellular retention [54]. This property was utilized by Bhatnagar and colleagues [50] for CAR-T cell radiolabeling and tracking. GNP were labeled with ^{64}Cu^{2+} using the macrocyclic chelator (1,4,7,10-tetraazacyclododecane-1,4,7,10-tetraacetic acid, DOTA) and polyethyleneglycol (PEG) 2000 to construct GNP-^{64}Cu/PEG2000, which was then electroporated into genetically modified CD19-targeting CAR-T cells by the *Sleeping Beauty* transposon/transposase system. The GNP-^{64}Cu/PEG2000-loaded CAR-T cells were infused intravenously into healthy mice for PET imaging, demonstrating intense activity accumulation in the lungs at 10 min post-infusion. Subsequently, activity in the liver and spleen gradually increased. Although

this study exhibited the feasibility of a nanomaterial-based strategy for *in vitro* labeling and *in vivo* imaging of CAR-T cells, it was limited to design an imaging strategy for tumor-bearing mice with T cell infusion and to provide information on whether T cells home to the tumor.

The abovementioned investigations confirm the feasibility of a direct labeling strategy for CAR-T migration detection in solid tumors. However, some inherent shortcomings hamper the clinical translation, including imaging signal dilution due to cell division and death, and signal aliasing due to dead labeled cells being consumed by phagocytes. Moreover, because a direct labeling strategy allows CAR-T cells to be radiolabeled only once *in vitro* before administration, radionuclides with relatively long half-lives, such as ^{64}Cu (12.7h), ^{111}In (67 h), and ^{89}Zr (78.4 h), would be preferred to extend the imaging period. Because a treatment cycle of CAR-T therapy usually lasts for several weeks [55, 56], even if the imaging timeframe of the direct labeling approach can reach 96 h [48] or 6 d [52] after probe infusion, it is still insufficient for longitudinal imaging and obtaining information about the *in vivo* kinetics of CAR-T cells in later parts of the treatment cycle. In addition, nanomaterials such as GNPs may need to be introduced into cells as carriers of the radionuclide. Whether or not they may cause potential biological toxicity to CAR-T cells is a question that requires careful consideration.
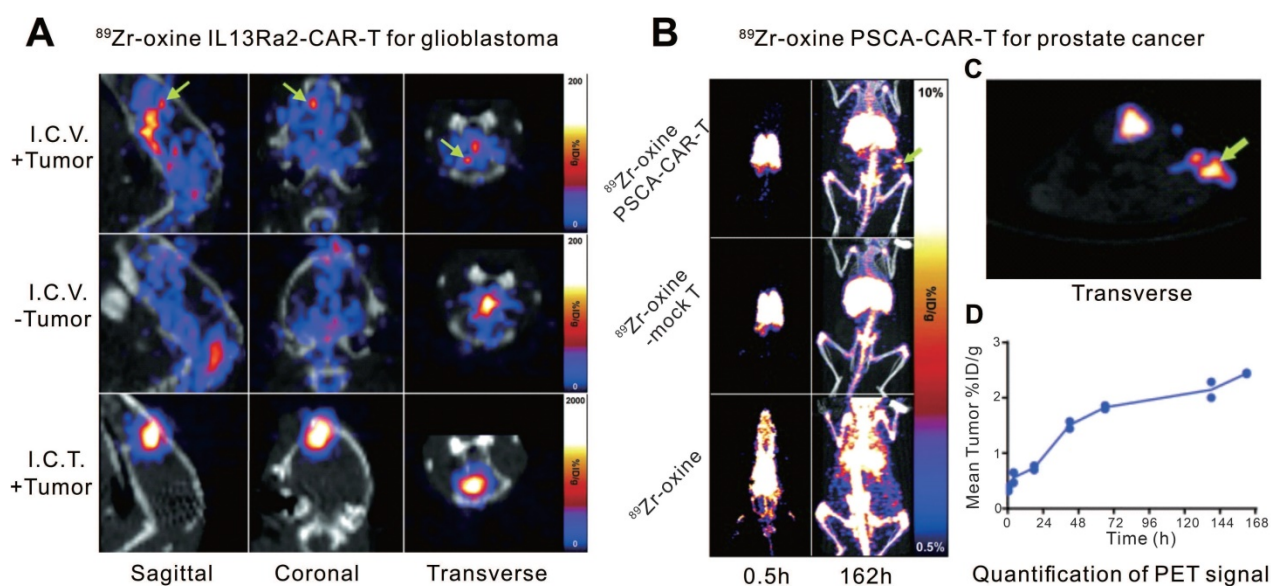

Figure 2. CAR-T cellular visualization based ^{89}Zr-oxine labeling. A. Mice with (+Tumor) or without (−Tumor) glioblastoma in the left cortex were administrated ^{89}Zr-oxine-labeled IL13Rα2-CAR-T cells injected into the cerebrospinal fluid via the right ventricle (I.C.V.) or directly into the tumor (I.C.T.). PET/CT images demonstrated activity accumulation in the tumor sites by I.C.V. (top row, green arrows) and I.C.T. (bottom row), whereas the activity is diffusely distributed in the ventricular system in tumor-free mice (middle row). **B.** Prostate cancer xenograft-bearing mice were treated with ^{89}Zr-oxine labeled PSCA-CAR T cells (top row), ^{89}Zr-oxine labeled untransduced T cells (middle row), and cell-free ^{89}Zr-oxine (bottom row), respectively. Pulmonary activity accumulation was observed in the mice treated with T cells, while the activity of the cell-free ^{89}Zr-oxine was rapidly distributed throughout the blood at the early time point. Activity in subcutaneous xenograft (green arrow) was detected in mice treated with CAR T cells but not with mock T cells or ^{89}Zr-oxine. **C.** The transverse image of subgraph B. **D.** Time-activity curve of the region of interest of xenografts in mice treated with ^{89}Zr-oxine PSCA-CAR T cells. Adapted with permission from [52], copyright 2018 Society of Nuclear Medicine and Molecular Imaging.

Reporter gene strategy

Compared to direct labeling, reporter gene imaging exhibits many advantages. First, genetic engineering and consequent stable genomic integration allow the reporter protein to be stably expressed in living transduced cells. Since dead cells no longer express the reporter gene product, the reporter probe will not bind to them, ensuring that all detected signals are from living cells [57]. Second, cell division does not cause signal loss or dilution because progeny CAR-T cells also express reporter protein. Third, the transduction of reporter genes does not affect the viability, proliferation, or tumor killing ability of T cells *in vitro* or *in vivo* [58, 59]. Fourth, the application of appropriate reporter/probe combinations can achieve repeated serial imaging without a restricted timeframe. Finally, based on the advantages of sequential imaging, radionuclides with shorter half-lives, such as ^{68}Ga (67 min) and ^{18}F (109.7 min) may be used for probe construction, therefore restricting ionizing radiation exposure to T cells and reducing potential radiation toxicity.

In light of these advantages, the reporter gene strategy has been used for ACT mapping and monitoring [41, 60-63]. Recently, researchers have applied this strategy to CAR-T. Because the engineering of CAR-T cells requires DNA transduction *in vitro*, some researchers construct a recombinant DNA to co-express a CAR for tumor-specific targeting, and a reporter for corresponding PET/SPECT probe binding and cellular imaging in animal models or clinical applications.

Enzyme-based reporter gene

The only reporter gene currently used for CAR-T imaging in human patients is an enzyme-based reporter gene, herpes simplex virus 1 thymidine kinase (HSV1-tk), which enables PET imaging with several radiolabeled probes such as ^{124}I/^{125}I/^{131}I/^{14}C-labeled 2-fluoro-2-deoxy-1-β-D-arabinofuranosyl-5-iodouracil (FIAU), ^{18}F labeled 9-(4-fluoro-3-hydroxy-methylbutyl)guanine (FHBG) [64, 65], 2'-deoxy-2'-fluoro-5- ethyl-1-β-D-arabinofuranosyl-uracil (FEAU) [66] and 9-(3-fluoro-1-hydroxy-2-propoxymethyl)-guanine (FHPG) [65, 67, 68]. HSV1-tk-based reporter gene imaging has been used to monitor the biodistribution and homing of various transduced cells, such as administrated cytotoxic T lymphocytes (CTLs) in tumor xenografts [69] and inflammation models [70], grafted neurons in brain injury [71], and transplanted stem cells in ischemic heart disease [72]. Dotti et al. [73] reported that infused sr39 mutant HSV-1 tk gene-transduced T lymphocytes could be visualized by ^{18}F-FEAU PET imaging in nonhuman primate models, which supports their potential application in humans. Ponomarev et al. have employed HSV1-tk reporter-based imaging to monitor the T-cell receptor (TCR)-dependent nuclear factor of activated T cells (NFAT)-mediated activation of T cells, which suggests that the monitoring of CAR-T cell activation can be achieved through HSV1-tk reporter-based imaging [74].

The first case using HSV-1 tk reporter gene imaging to visualize administered CAR-T cells was of a 57-year-old man with grade IV glioblastoma multiforme (NCT00730613), reported by Yaghoubi et al. [64] After gross tumor resection, a cumulative dose of 1×10^9 therapeutic T cells (expressing HSV1-tk as the reporter gene, and interleukin 13 [IL-13] zetakine targeting for IL-13Ra2-expressing tumor) into the tumor site. The ^{18}F-FHBG PET/MR images demonstrated activity trapped both in the surgically resected tumor bed and in unresected tumor (**Figure 3, A-C**), which was thought to correspond to T cells accumulation. This case suggests that ^{18}F–FHBG can accumulate within glioma tumors [75], and should be able to detect transferred cells that express HSV1-tk. However, because of the lack of a critical baseline PET image before CAR-T cells injection, the authors could not confirm whether the ^{18}F-FHBG activity in the tumor region originated from the CAR-T cells *per se* or from tumor-associated nonspecific uptake [76].

Based on these findings, Yaghoubi's group conducted a clinical trial (NCT00730613 & NCT01082926) with the same reporter imaging approach, which involved seven cases of recurrent high-grade glioma that were resistant to conventional therapies [77]. The results showed that the total lesion ^{18}F-FHBG activity (SUV$_{mean}$ × volume of interest) in sites of tumor recurrence significantly increased on the post-CTLs PET scan compared with the pre-CTLs PET scan, which suggested CAR-T cells migrating to the tumor sites (**Figure 3D-E**). The work from Yaghoubi et al. lays the foundation for a reporter gene imaging strategy to monitor CAR-T therapy of solid tumors in clinical practice. One important limitation of the presented system is the uptake of ^{18}F-FHBG in untreated tumors and tumor resection sites. Yaghoubi et al. explained that the retention of ^{18}F-FHBG in tumors before CTLs infusion may result from slow washout of the radiotracer from the resection cavity or be a consequence of off-target retention in the tumor cells [77]. This accumulation of radiotracer in the untreated tumors or the tumor resection sites pre-CTLs infusion does cause potential background interference, which makes it difficult to quantify the truly signal emitted from transduced T cells after CTLs infusion. Although the reporter gene imaging with HSV1-tk and its mutant has been introduced into

the clinical trials, the potential immunogenicity poses a major risk. Using mammalian species reporter gene constructs could effectively reduce this risk [78, 79].

In addition to clinical trials, a few recent studies have used reporter gene strategy for PET/SPECT imaging to verify the feasibility of tracking CAR-T cells in animal models (**Table 1**). Sellmyer's group developed a high-sensitivity PET reporter/probe pair, *E. coli* dihydrofolate reductase (eDHFR) and ^{11}C/^{18}F-fluoropropyl-trimethoprim (TMP) [80, 81]. TMP, the probe precursor of this reporter system, is an inexpensive and widely available anti-biotice with and established toxicity profile. The absorption, distribution, metabolism, and excretion of TMP are favorable with a relatively short blood half-life in humans, and it has a low serum protein binding ratio (approximately 50%) [82, 83]. The previous work on ^{11}C-TMP [80] showed this reporter system to have high sensitivity for visualizing transduced cells, which can detect as few as 3×10^5 cells. Sellmyer et al. applied reporter imaging strategy to monitor CAR-T

cells targeted to the GD2 disialoganglioside in murine osteosarcoma models [84]. ^{18}F-TMP PET/CT showed promising accumulation in eDHFR$^+$ human colon carcinoma (HCT116) cell xenografts with physiologic uptake in the liver, kidneys, and intestines, whereas lower uptake was noted in the control eDHFR$^-$ tumor, blood pool, heart, lungs, muscles, spleen, skin, and the brain [84]. The GD2$^+$ tumor-harboring mice were administered with eDHFR-expressing anti-GD2 CAR-T cells, and ^{18}F-TMP PET/CT was performed to track the cells. The results illustrated the CAR-T cells mainly accumulate in the spleen at the early time point, and migrate to the tumor at the late time point. These findings provide temporal and spatial information for homing and infiltration of T cells. Notably, eDHFR is a smaller protein compared with HSV-tk (18 kDa *versus* 46 kDa) with fewer immunologically active epitopes measured by sequencing. Future studies might focus on modifications of the eDHFR/TMP complex to enhance the binding affinity and humanize or
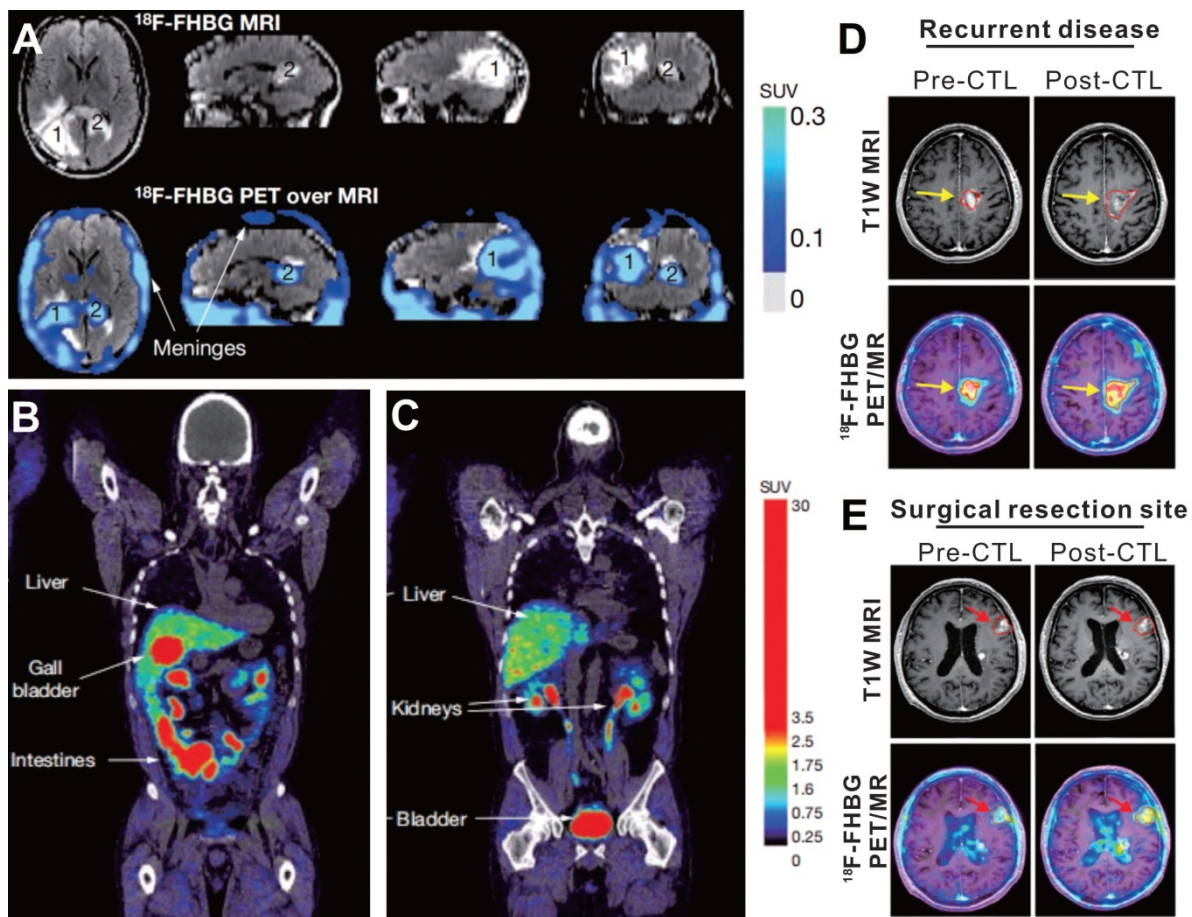

Figure 3. ^{18}**F-FHBG PET imaging based on HSV-1 tk reporter enables CAR-T cell visualization in patients with glioblastoma. A.** Images of brain MRI and ^{18}F-FHBG PET/MRI superposition in a patient who received IL-13- and HSV-1 tk- expressing T cells. Both the surgically resected tumor site (lesion 1, which received CAR-T injection) and the unresected tumor (lesion 2, which did not receive CAR-T injection) had higher activity in contrast to the normal brain background. **B-C.** Sites of physiologic uptake of ^{18}F-FHBG PET/CT included the liver, gallbladder, intestines, kidneys, and bladder. **D-E.** Pre- and Post-CTLs ^{18}F-FHBG PET/MR images in recurrent disease (**D**, received CAR-T injection) and at untreated tumor (**E**) sites in a 60-year-old man with multifocal left hemispheric glioma. ^{18}F-FHBG PET images showed the recurrent tumor and untreated tumor (B2, red arrows) had obvious activity that increased after CTLs treatment. A-C adapted with permission from [64], copyright 2008 Springer Nature, and D-E from [77], copyright 2017 American Association for the Advancement of Science.

truncate the enzyme to minimize its potential immunogenicity, which could offer important advantages in terms of deepening the understanding of CAR-T kinetics and promoting clinical translation [85, 86].

Symporter-based reporter gene

Human sodium-iodine symporter (hNIS) belongs to the sodium-dependent transporter family, which regulates the transmembrane transport of iodide and several other anions [87, 88]. The hNIS is endogenously expressed in the thyroid and some other extra-thyroidal tissues including the gastric mucosa, salivary glands, and lactating mammary glands [89-91]. In addition, hNIS is non-immunogenic, and is not internalized upon substrate uptake [92]. Moreover, hNIS reporter imaging is suitable for PET and SPECT because NIS-expressing cells can effectively and specifically accumulate various radionuclides including ^{99m}Tc, ^{123}I, ^{124}I, and ^{131}I [90, 93]. As an imaging reporter gene, hNIS has been well-used in tracking or assessing immune cells [94-96], regenerative cells [97-99], tumor cells [100-102], and cellular therapies [58, 103] in animal

studies and clinical trials. Based on these attributes, the hNIS is a promising reporter gene with the potential for visualizing and assessing CAR-T cells. Emami-Shahri and colleagues [58] used an hNIS/^{99m}TcO$_4^-$ reporter gene/probe pair for imaging and monitoring prostate-specific membrane antigen (PSMA)-targeting CAR-T cells. They transduced hNIS into specific PSMA-targeting CAR-T (4P28ζN$^+$) cells, which did not reduce their expression of CAR, and did not interfere with their efficient killing properties against the PSMA-overexpressing prostate cancer cell line PC-LN-PSMA *in vitro* as well as against tumor-bearing mice *in vivo*. Serial SPECT/CT imaging for 4P28ζN$^+$ or control (4PTrN$^+$, non-PSMA-targeting) T cells in tumor-bearing mice was performed over 14 d p.t, showing increased ^{99m}TcO4$^-$ activity in tumors treated with 4P28ζN$^+$ T cells and no significantly increased signal in tumors treated with 4PTrN$^+$ T cells. These data not only provided evidence that T cells could migrate to the tumor and infiltrate tumor tissue, but that specific CAR-T cells targeting PSMA have stronger tumor homing ability in comparison to control CAR-T cells (**Figure 5**).
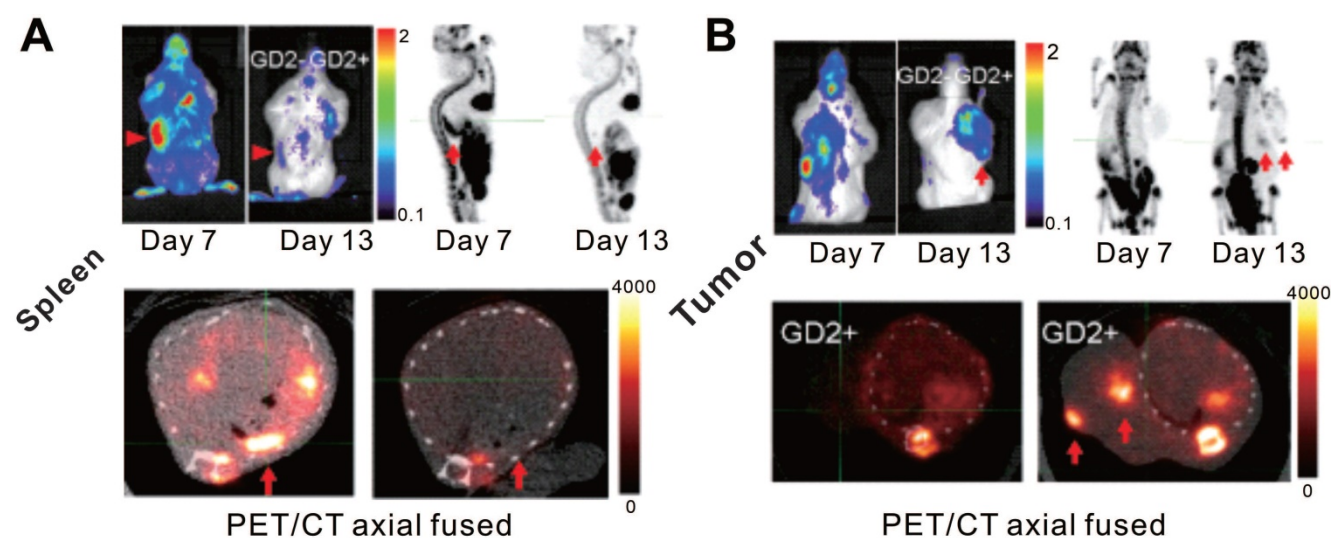

Figure 4. CAR-T cellular visualization based on eDHFR reporter imaging. After receiving eDHFR-expressing anti-GD2 CAR-T cells, mice bearing both GD2$^-$ HCT116 (left shoulder) and GD2$^+$ 143b tumor (right shoulder) were imaged with BLI and ^{18}F-TMP PET for CAR-T cellular visualization. The images showed elevated BLI and PET signal in the spleen on day 7 post T cells infusion (p.t), which decreased on day 13 p.t (**A**, red arrows). Neither GD2$^-$ nor GD2$^+$ tumor displayed BLI or PET signal on day 7 p.t, whereas increased BLI and PET signal was detected only in GD2$^+$ tumor (**B**, red arrows) on day 13 p.t. Adapted with permission from [84], copyright 2019 The American Society of Gene and Cell Therapy.

Table 1. CAR-T imaging in animal models based on reporter gene strategy

Reporter	Reporter type	Probe & Dose	CAR-targeting	CAR-T infused dose	Transduction method	Tumor cell line	Tumor modeling (inoculated tumor cells number, modeling route)	Imaging Modality	Detection limit (cell number)	CAR-T detection (time)	Ref.
eDHFR	Enzyme-based	^{18}F-TMP 3.7 MBq	GD2	1×10^6	Lentivirus vector	143b (human osteosarcoma)	10×10^6 cells Subcutaneous xenograft	PET/CT	11,000*	Up to 13 d p.t**	[84]
hNIS	Symporter-based	^{99m}TcO$_4^-$ 20MBq	PSMA	1×10^6	Lentivirus vector	PC-LN3-PSM (prostate cancer)	2.5×10^5 cells Subcutaneous xenograft	SPECT/CT	15,000	Up to 14 d p.t	[58]
hNIS	Symporter-based	^{18}F-BF$_4^-$ 5 MBq	Pan-ErbB	5×10^6	Lentivirus vector	MDA-MB-436 & MDA-MB-231 (triple	1×10^6 cells Orthotopic mammary xenograft	PET/CT	3,000	Up to 14 and 15 d p.t***	[105]

Reporter	Reporter type	Probe & Dose	CAR-targeting	CAR-T infused dose	Transduction method	Tumor cell line	Tumor modeling (inoculated tumor cells number, modeling route)	Imaging Modality	Detection limit (cell number)	CAR-T detection (time)	Ref.
						negative breast cancer)					
SSTR-2	Receptor-based	^{68}Ga-DOTATOC#	ICAM-1	2-3×10⁶	Lentivirus vector	8505C (thyroid cancer)	1×10⁶ cells Tail intravenous Primary lung tumor & hepatic/distant metastases	PET/CT	50,000	Up to 27 d p.m.##	[109]
tPSMA$^{(N9del)}$	Receptor-based	^{18}F-DCFPyL 14.8 MBq	CD19	2×10⁶	Lentivirus vector	Nalm6 (acute lymphoblastic leukemia)	1×10⁶ cells Subcutaneous xenograft	PET/CT	2,000	Up to 12 d p.t	[59]
DAbR1	Antibody-based	^{86}Y-AABD 3.7 MBq ^{177}Lu-AABD 37 MBq	CD-19	3×10⁶	Retrovirus	Nalm6 (acute lymphoblastic leukemia)	5×10⁶ cells Subcutaneous xenograft	PET/CT SPECT/CT	Not available	4h, 16 h p.t 4h, 20 h p.t	[125]

*The detection limit is 11,000 cells/mm³; **p.t: post T cells infusion; ***: 14 d p.t for MDA-MB-436 xenografts, and 15 d p.t for MDA-MB-231 xenografts; #: the dose of ^{68}Ga-DOTATOC is not available; ##p.m.: post modeling.
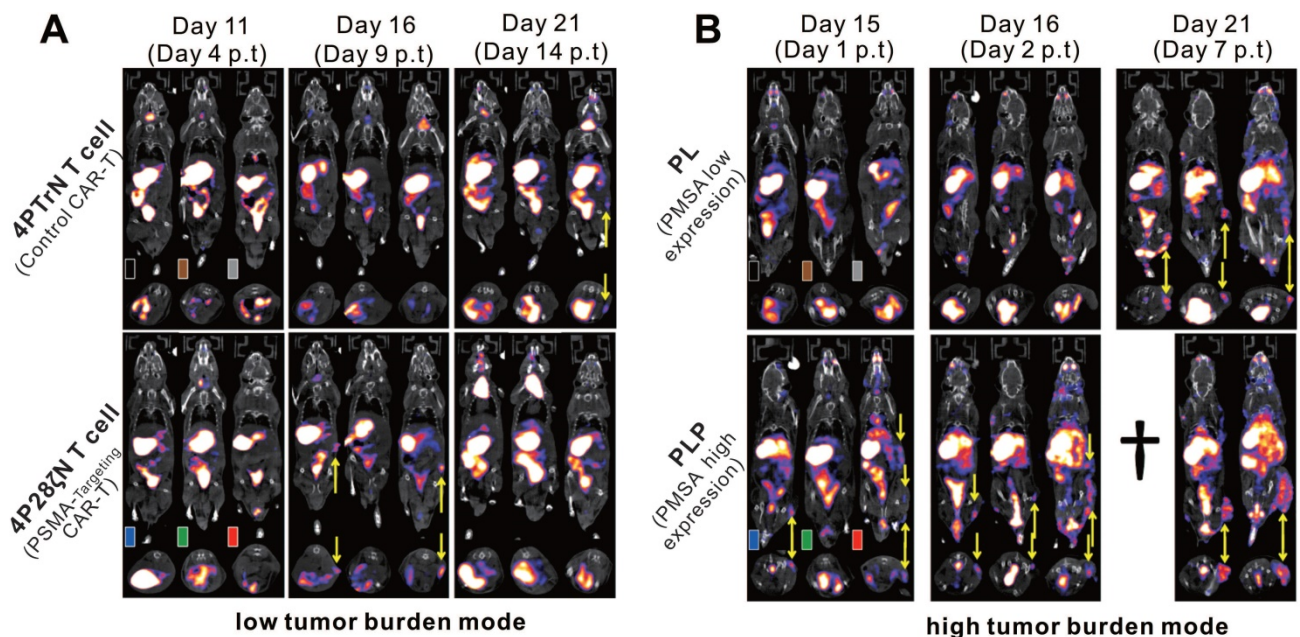

Figure 5. CAR-T cellular visualization based on hNIS reporter SPECT/CT imaging. A. ^{99m}TcO$_4^-$ SPECT images of low tumor burden mice (imaged 7 d post tumor inoculation). Mice with PC-LN3-PSMA (PLP) cell subcutaneous xenograft were treated with control CAR-T (4PTrN⁺, upper row) cells and PSMA-targeting CAR-T (4P28ζN⁺, lower row) cells. No visible activity was detected in the tumors of all of the three control mice on the day 4 p.t and day 9 p.t, and only one had subtle activity in the tumor on the day 14 p.t. Although there is no detailed description in the original reference, the accumulation in the tumor (yellow arrows) of rightmost mouse on day 14 p.t might be due to the non-specific infiltration of T cells into tumor tissue [104]. In comparison, significant SPECT signal was detected in the tumor of the mice treated with 4P28ζN⁺ CAR-T cells on day 9 p.t, and then the signal decreased on day 14 p.t as the tumor regression. **B**. ^{99m}TcO$_4^-$ SPECT images of high tumor burden mice (imaged 14 d post tumor inoculation). Mice with PC-LN3(PL) cell xenograft (upper row) and PC-LN3-PSMA (PLP) cell xenograft (lower row) received 4P28ζN⁺ CAR-T cell infusion. Only subtle activity was detected on day 7 p.t in the PL tumors, indicating only a few CAR-T cells infiltration. In contrast, obvious SPECT signal was noted in the PLP tumors as early as day 1 p.t, which enhanced constantly till day **7** p.t (†=dead mouse). Adapted with permission from [58], copyright 2018 Springer Nature.

Volpe et al. used the PET probe ^{18}F-BF4$^-$ to reaffirm the role of the NIS reporter system in trafficking CAR-T cells [105]. They constructed T4NT CAR-T cells that express the NIS reporter and can target the pan-ErbB family. The cell uptake assay showed that the CAR-T cells had significantly higher *in vitro* uptake of SPECT radiotracer ^{99m}TcO4$^-$ and PET radiotracer ^{18}F-BF4$^-$ in comparison to NIS-free T cells. And after radiation exposure, the cellular viability, IFN-γ secretion ability and tumor killing ability of CAR-T cells were not significantly affected. Notably, the researchers observed that when CAR-T cells exposed to radioactive probes, large doses of ^{99m}TcO4$^-$ (>51mBq/cell) and ^{18}F-BF4$^-$ (>14mBq/cell) will induce DNA damage in the early stage (at 2h), but radiation-induced damage was repaired within 24 h. Two orthotopic triple-negative breast cancer (MDA-MB-436 and MDA-MB-231)-bearing NSG mice received 5 × 10⁶ T4NT CAR-T cells by intratumoral injections, and then underwent serial small animal PET/CT imaging (on day 1, 7, and 15 p.t for MDA-MB-436; on day 1, 5, 14 for MDA-MB-231). Surprisingly, CAR-T retention was observed in MDA-MB-436 xenografts up to the day 15 p.t, whereas CAR-T cells in MDA-MB-231 xenografts disappeared over that time (**Figure 6A-D**). The author believes that this difference in

CAR-T retention is likely to be intrinsic to the tumor cells, that is, from the influence of immune checkpoints. They further detected the expression of programmed death ligand 1 (PD-L1) in the two tumors, and an inverse correlation between T4NT CAR-T cell retention and the immune checkpoint inhibitor PD-L1 expression was observed (**Figure 6E**). This study achieved PET-based NIS reporter gene imaging with a higher detection sensitivity comparing to the aforementioned SPECT imaging (3,000 cells *versus* 15,000 cells) [58]. They concluded that immune checkpoints affect CAR-T cells retention in different tumors, and highlighted the multifactorial challenges facing CAR-T therapy in solid tumors.

Receptor-based reporter gene

Somatostatin receptors (SSTRs) belong to the G protein-coupled receptor family, which are highly conserved in mice and humans with relative low expression in most organs. SSTRs contain five distinct subtypes (termed SSTR1, 2, 3, 4, and 5). SSTR2 exhibits the highest affinity for natural somatostatin and synthetic somatostatin analogs [106, 107]. A major advantage of the SSTR2 reporter system is its compatibility with multiple probes such as [68]Ga

labeled 1,4,7,10-tetraazacyclododecane-N[I], N[II], N[III], N[IIII]-tetraacetic acid-d-Phe[1]-Tyr[3]-octreotate (DOTATATE) and 1,4,7,10-tetraazacyclododecane-N[I], N[II], N[III], N[IIII]-tetraacetic acid (D)-Phe[1]-thy[3]-octreotide (DOTATOC) for PET and ^{99m}Tc-Hynic-octreotide for SPECT [108]. Vedvyas et al. engineered native human T cells to co-express intercellular adhesion molecule-1 (ICAM-1) for tumor targeting and SSTR2 for reporting [109]. The authors established a simple method for estimating the density of SSTR2-expressing CAR-T cells infiltrating in solid tumors (**Figure 7**). Interestingly, the authors revealed a biphasic CAR-T cell expansion and contraction pattern in the survivors, almost matching tumor growth and destruction, whereas the non-survivors had unabated T cell expansion because the tumor-killing effect of the CAR-T cells could not overcome more intense tumor growth. Although this study provides a visual tool for quantifying T cell infiltration and assessment of prognosis basing on SSTR2 reporter gene imaging, several shortcomings of this reporter system need to be mentioned: i) SSTR2 receptor is expressed endogenously on various immune cell types including T-cells, B-cells and macrophages, decreasing the reporter imaging specificity and
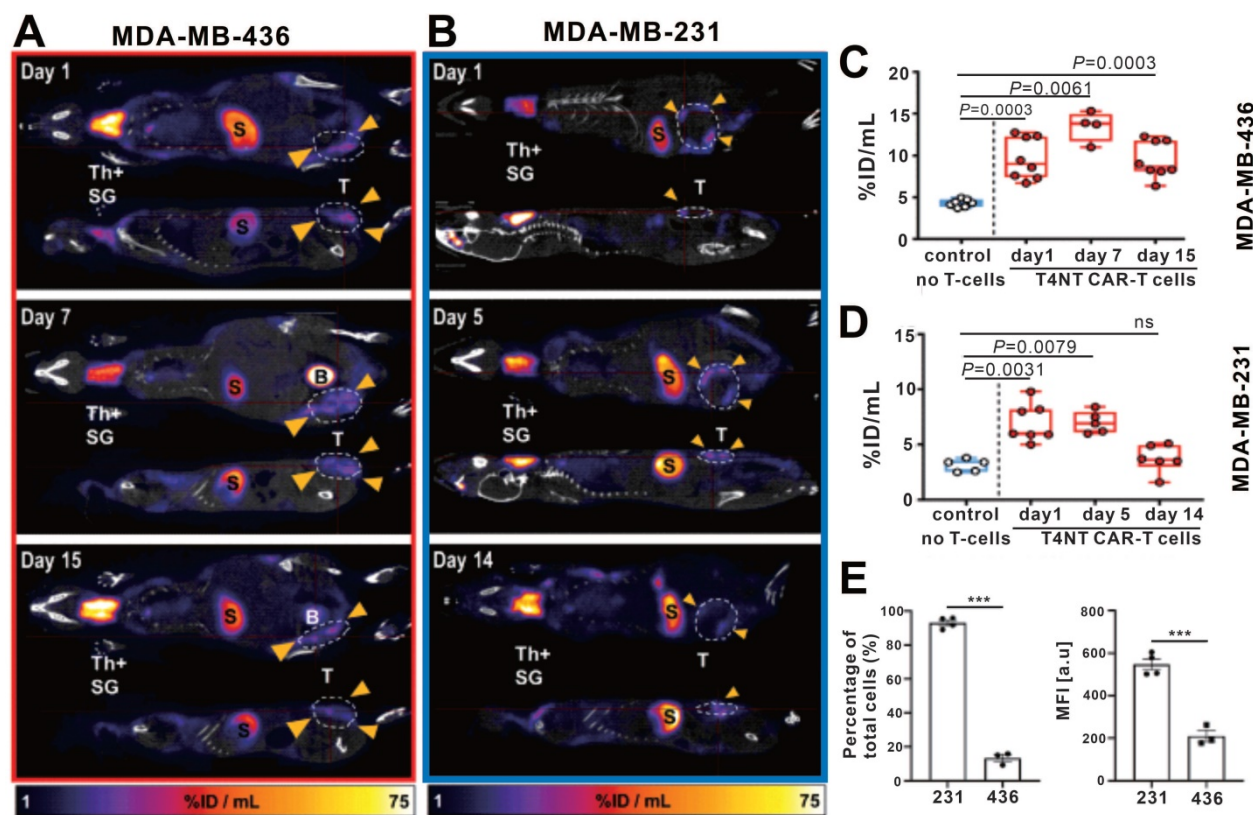

Figure 6. CAR-T retention in tumor visualized on hNIS reporter imaging. A-B: ^{18}F-BF4- PET/CT imaging of MDA-MB-436 and MDA-MB-231 xenograft-bearing mice. **C-D**: The PET signal intensity of the ROI of the MDA-MB-436 and MDA-MB-231 xenografts. Physiological uptake in the thyroid (Th+), salivary glands (SG), stomach (S), and bladder (S) on PET/CT images was noted in both MDA-MB-436 and MDA-MB-231 xenograft-bearing mice. The CAR-T retention in tumor (circles and arrowheads) differed: CAR-T signal was always observed in MDA-MB-436 xenografts (**A**), and remained at a high level until day 15 p.t (**C**); while the CAR-T signal in MDA-MB-231 xenografts decreased over time (**B** and **D**). **E.** Significantly higher PD-L1 expression in MDA-MB-231 compared with MDA-MB-436 cells was observed. Adapted with permission from [105], copyright 2020 The American Society of Gene and Cell Therapy.

possibly interfering with immune function [107, 110, 111]; ii) it is also expressed in the gastrointestinal tract; and iii) the SSTR2 receptor will be internalized upon ligand binding [108, 112].

PSMA is a non-immunogenic human protein whose tissue expression is normally restricted to a few organs such as the prostate, kidneys, and brain [113, 114]; it is a widely used target for various imaging modalities [115, 116]. However, internalization of wild-type PSMA upon ligand binding prevents its clinical translation as a reporter gene. An N-terminally modified PSMA variant, tPSMA[(N9del)],

was designed by Il Minn and colleagues to prevent PSMA internalization and increase surface expression [117], which enhanced the binding and overall imaging sensitivity of the PET probe 2-(3-{1-carboxy-5-[(6-[18F]-fluoro-pyridine-3-carbonyl)-amino]-pentyl} F-ureido)-pentanedioic acid ([18F]-DCFPyL). Il Minn et al. also recently applied the tPSMA[(N9del)]/[18F]-DCFPyL pair for CD19-targeting CAR-T monitoring [59]. [18F]-DCFPyL exhibited effective binding to PSMA because of the high number of target sites per cell (approximately 1×10^6), enabling the visualization of as few as 2000 cells *in vitro* or *in vivo* (**Figure 8A-B**).
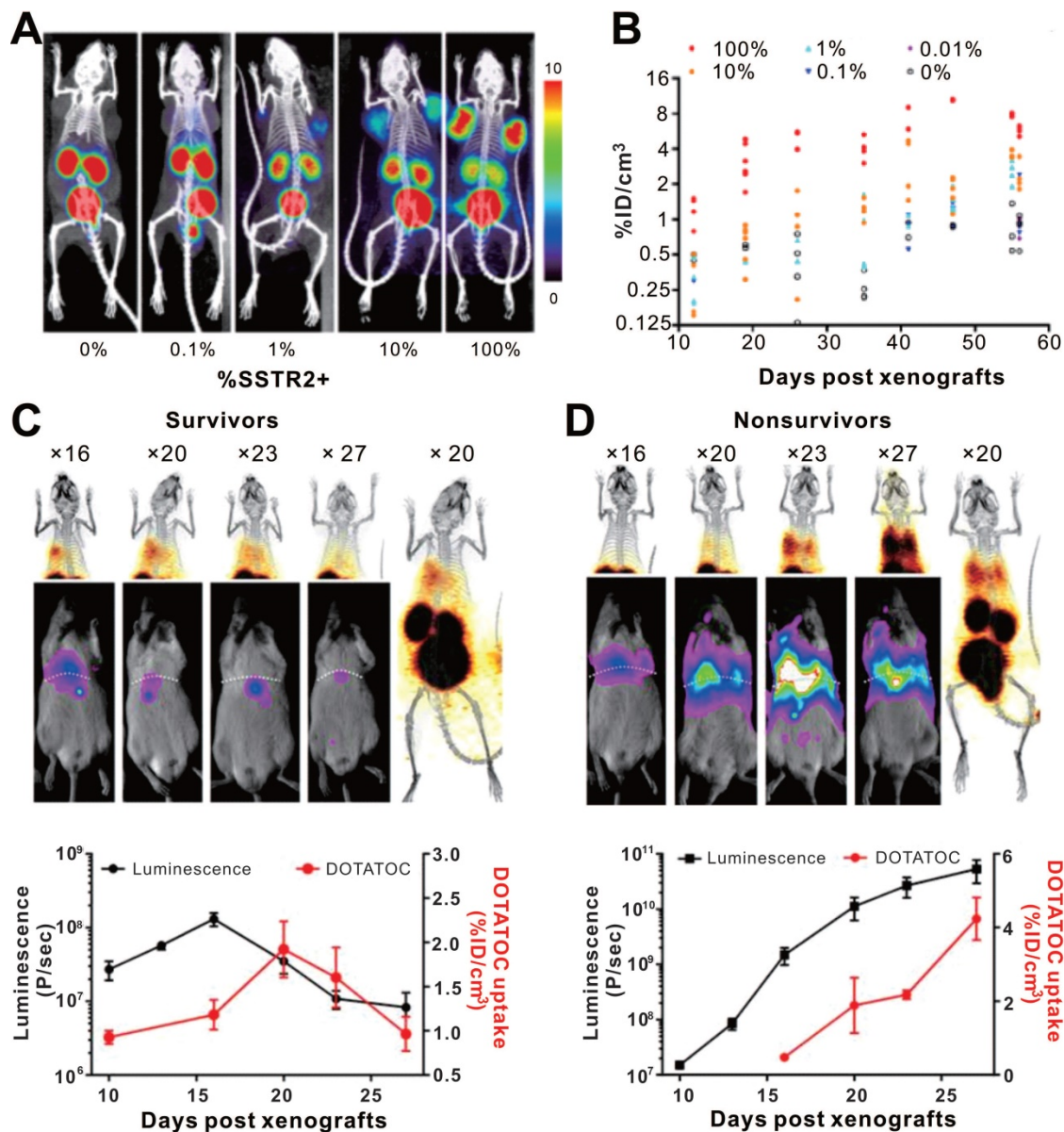

Figure 7. CAR-T cellular visualization based on SSTR reporter imaging. A-B. SSTR2+ CAR-T cell detection limit of [68Ga]-DOTATOC PET/CT. Jurkat T cell clusters mixed with different proportion of CAR-T cells were inoculated into the shoulders of NSG mice, which were imaged with [68Ga]-DOTATOC PET/CT. As low as a 1% SSTR2+ CAR-T cell cluster was visible (A), and the [68Ga]-DOTATOC uptake increased following cell proportion increase and over time (B). **C-D.** Serial BLI/PET images (upper row) and corresponding time-signal curves (bottom row) of survival (left column) and non-survival (right column) mice with 8505c-FLuc+GFP+ cells *in situ* lung tumor after SSTR2+ ICAM-1-targeting CAR-T treatment (the labels "× 16, 20, 23…" refer to the day 16, 20, 23…post xenograft modeling). The survivors' images exhibited an increase in uptake followed by a decline. Conversely, the BLI and PET signals continually increased in non-survivors. Adapted with permission from [109], copyright 2016 American Society for Clinical Investigation.

This detection limit provides the potential to track the kinetics of a small number of CAR-T cells. The authors established subcutaneous xenografts and osseous metastases in NSG mice by inoculating them with CD19+ Nalm6 cells. They performed serial ^{18}F-DCFPyL PET/CT imaging to visualize CD19 CAR-T infiltration in local and metastatic tumors (**Figure 8C-F**). They also showed that the number of CAR-T cells in the peripheral blood and bone marrow did not correlate with the number of cells infiltrating the tumors, indicating that both peripheral blood tests and bone marrow biopsies may not truly reflect the extent of CAR-T tumor infiltration.

In addition to the aforementioned SSTR2, hNIS, HSV1-tk, and PSMA, another human reporter gene, human norepinephrine transporter (hNET) has been used for T cell visualization [118]. The advantage of hNET as a reporter is that its corresponding radiolabeled probe, metaiodobenzylguanidine (MIBG), is currently used in the clinic, and can be radiolabeled with ^{123}I or ^{131}I for SPECT and γ-camera imaging and with^{124}I for PET imaging [119-121]. A comparative study [62] to investigate the sensitivity of four different reporter gene systems (HSV1-tk, hNET, hNIS, and human deoxycytidine kinase double mutant [hdCKDM]) in detecting reporter transduced T cells showed that the hNET reporter system is the most sensitive and capable of detecting approximately $3.5\text{-}4.0 \times 10^4$ T cells at the site of T cell injection in mice. This makes it a potential candidate for CAR-T visualization; whether it has clinical translation potential will require further experimental data.
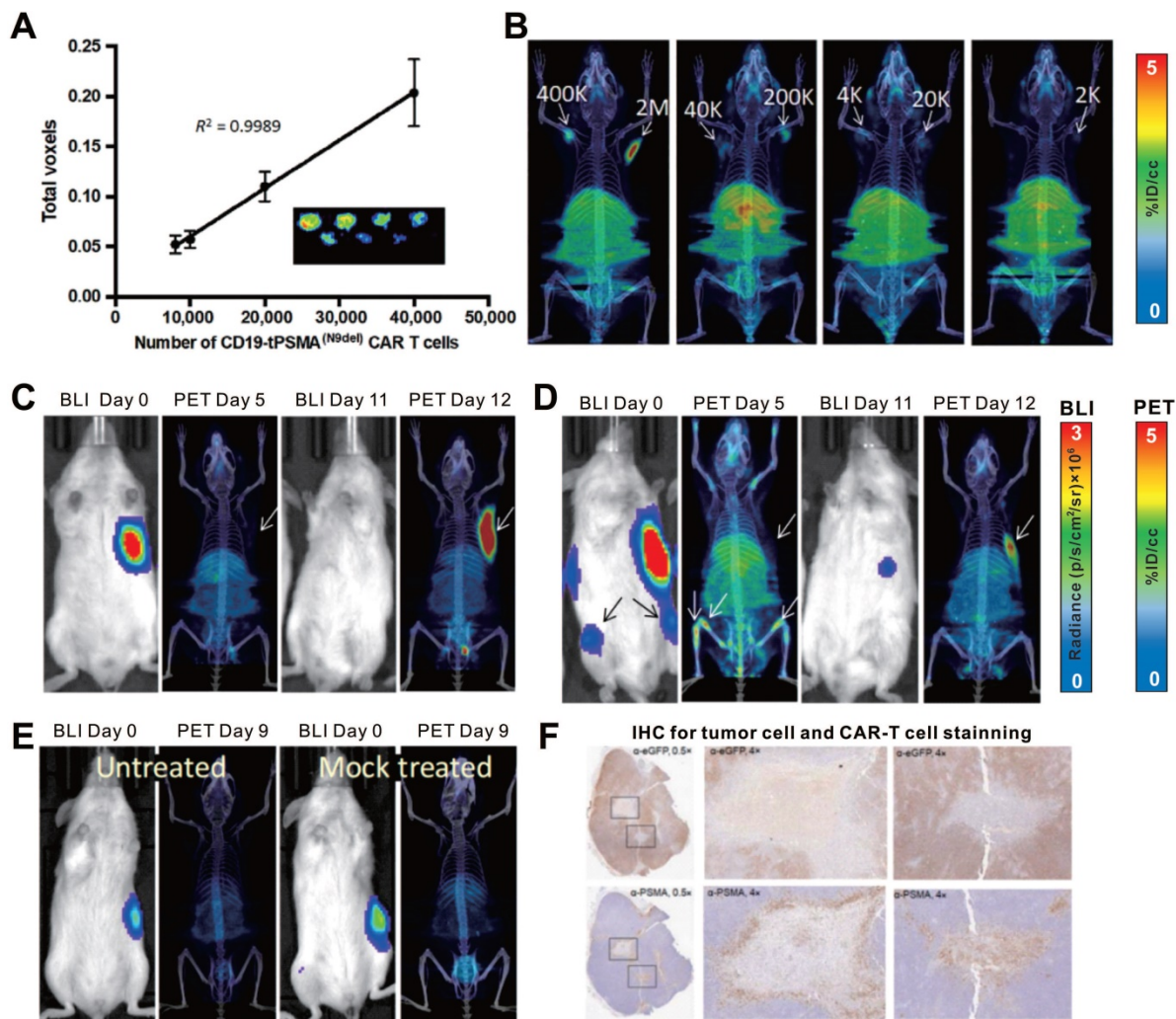

Figure 8. CAR-T cellular visualization based on PSMA reporter imaging. A-B. The *in vitro* (A) and *in vivo* (B) detection limit of ^{18}F-DCFPyL for CD19-tPSMA CAR-T cells. **C-E.** NSG mice with CD19+Nalm6-enhanced green fluorescent protein (eGFP)-fLuc xenograft at the right frank (C, D, and E) and bone metastases (D) were treated with CD19-tPSMA CAR-T cells (C, D), untransduced T cells (E, right panel), and no cells treated (E, left panel), and then underwent BLI for visualization of tumor cells and ^{18}F-DCFPyL PET/CT for T cells alternately. The initial BLI confirmed tumor burden, and PET/CT in the early stage showed no observable signal in the xenograft; the PET/CT on the day 12 p.t exhibited CAR-T cells infiltration following by tumor regression (C). There was no significant PET signal in the subcutaneous xenograft whereas activity was detected in the bone metastases on the day 5 p.t; repeated BLI showed only subcutaneous remnant, with elevated PET signal accumulation (D). No PET signal was detected in the tumors, either in mice treated with mock T cells or in untreated mice (E). **F.** IHC confirmed CD19-tPSMA CAR-T cells infiltrating the xenograft. Adapted with permission from [59], copyright 2018 American Association for the Advancement of Science.
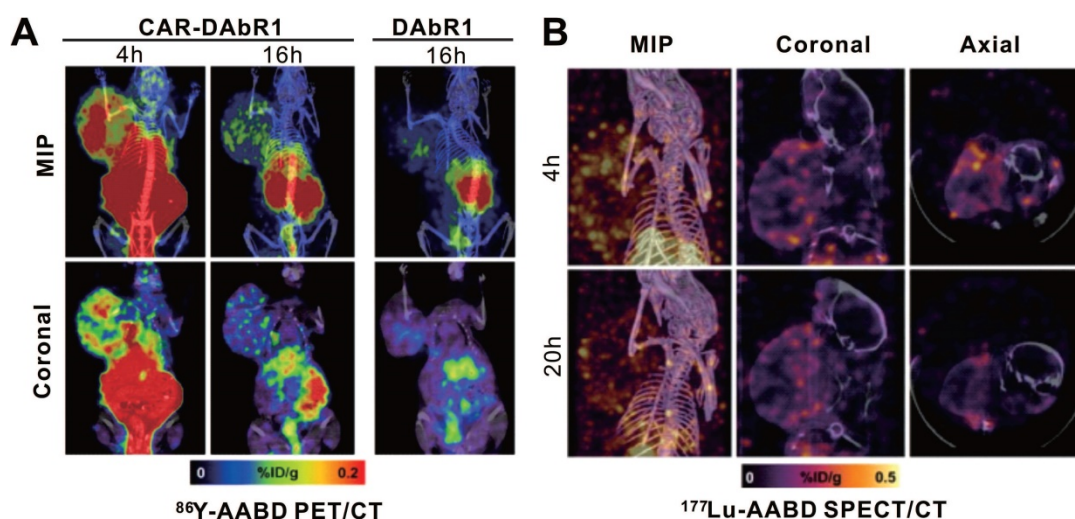
Figure 9. CAR-T cellular visualization based on DAbR1 reporter imaging. A. Adoptively transferred T cells tracking by [86]Y-AABD PET/CT. Maximum intensity projection (MIP) images (top row) and selected coronal (bottom row) images showed significant activity accumulation in tumors treated with CAR-DAbR1 T cells whereas no uptake observed in tumors treated with DAbR1 T cells. **B.** Transferred T cells tracking by ^{177}Lu-AABD SPECT/CT. MIP, coronal, and axial SPECT/CT images of tumor-bearing mice demonstrated the CAR-DAbR1 T cells localized in the tumors. Adapted with permission from [125], copyright 2018 Society of Nuclear Medicine and Molecular Imaging.

Antibody-based reporter genes

Krebs and colleagues used a murine-derived single-chain antibody variable fragment (scFv) fragment to construct 1,4,7,10-tetraazacyclododecane-1,4,7,10-tetraacetic acid (DOTA) antibody reporter 1 (DAbR1) as a reporter, based on previous work [122-124]. It can bind irreversibly to lanthanoid-(S)-2-(4-acrylamidobenzyl)-DOTA (AABD). Krebs et al. [125] used DAbR1/AABD as a reporter/probe pair for CD19-targeting CAR-T cells tracking *in vivo*. The authors labeled AABD with [86]Y and ^{177}Lu for PET/CT and SPECT/CT imaging, respectively. They first verified the feasibility of [86]Y-AABD PET/CT to visualize DAbR1-expressing CAR-T cells, then showed that whether the T cells were infused subcutaneously or intratumorally into subcutaneous U373 glioma xenografts, obvious PET signal emitted by CAR-T cells was noted. Mice with Nalm6 subcutaneous xenografts were treated with DAbR1-transduced, CAR-DAbR1-transduced, and non-transduced T cells, respectively. Both PET and SPECT showed that CAR-DAbR1 T cells aggregated in the high-CD19-expression tumors with favorable biodistribution and high image contrast, indicating the DAbR1 reporter imaging with PET/SPECT can localize and track CAR-T cells (**Figure 9**). The authors assessed the absorbed dose to T cells as approximately 20 cGy following a dose of 3.7 MBq of [86]Y-AABD administration, significantly below the previously reported tolerated dose (830 cGy) [126], which shows the safety of long-term monitoring of CAR-T cells using these radiotracers. In addition, considering the potentially lethal side effects of adoptively transferred CAR-T cells, the authors also explored DAbR1 as a suicide gene. They stated that the CAR-T cell cluster might receive an absorbed dose of 1.1 Gy/MBq following ^{177}Lu-AABD injection, which is a radiotoxic dose, indicating that T cells would be damaged or killed by the radiation.

The ideal reporter system for imaging should meet several conditions: (1) reporter gene expression should be low in normal tissues to avoid background interference and to obtain a good signal-to-noise ratio; (2) reporter-encoded products should have high specificity and affinity for the probe to improve imaging sensitivity and specificity; (3) the products should not be immunogenic, to avoid the risk of transduced T cells being attacked and cleared by the immune system; (4) a reporter should not affect the viability and function of engineered cells; and (5) it should have the ability to be imaged using a readily-available radionuclide with a clinical imaging modality. The reporter systems currently used for CAR-T therapy monitoring have one or more limitations, including the potential immunogenicity of HSV-1 tk, eDFHR, and DAbR1; and inherent expression in multiple normal organs resulting in background interference such as the case with SSTR2, hNIS, and PSMA. In addition, the reporter gene strategy has several common disadvantages, including complexity and difficulty in design and operation, promoter silencing, and potential mutation caused by DNA modification [127, 128]. In summary, reporter gene imaging can non-invasively visualize and monitor CAR-T cells *in vivo* with a relatively unrestricted time window, which is undoubtedly the most promising technique for clinical translation. Several key points require the most attention, that is, the safety, imaging sensitivity and specificity, the selection of an appropriate reporter system, and a protocol designed to address actual clinical issues.

Endogenous cell imaging methods

Another imaging strategy, endogenous T cell imaging, can map cell distribution *in vivo* and reflect cellular activation and functional status. To date, it is the most mature technology implemented in clinical research [35, 46]. Although there are few CAR-T-related studies in this field so far, it provides an alternative approach for *in vivo* imaging of CAR-T cells, which can be used as a supplement to direct labeling and reporter gene-based cellular imaging strategies.

Cell surface marker-based imaging

Cell surface markers are meaningful targets for *in vivo* imaging of specific T cell populations. These targets include general markers such as CD4, CD8, CD3, and immune checkpoints such as programmed death 1 (PD-1), PD-L1, and cytotoxic T-lymphocyte-associated protein 4 (CTLA-4) [129]. By constructing radionuclide probes that can specifically target these markers, PET/SPECT imaging can be used to trace target cell populations, evaluate the expression level of their markers, and reflect immune status. The construction of corresponding probes is based on the radiolabeling of antibodies or antibody-derived constructs and engineering bivalent antibody fragments, which build upon scFv derived from intact antibody, such as cys-diabodies (dimer of scFv) and minibodies (dimer of scFv-C_H3) [46, 130, 131].

Larimer et al. [132] used a murine [89]Zr-labeled anti-CD3 antibody ([89]Zr-DFO-CD3) to quantify T cell infiltration in colon cancer during anti-CTLA-4 treatment. High levels of infiltration were found to precede tumor regression. Rashidian et al. [133] developed an [89]Zr-labeled PEGylated single-domain antibody fragment specific for CD8, which detected CD8^{+} tumor-infiltrating lymphocytes in melanoma and pancreatic cancers, and distinguished therapy-responsive *versus* nonresponsive tumors tissue through longitudinal immunoPET. In preclinical models, both [89]Zr-labeled anti-CD4 and anti-CD8 cys-diabodies have been used to target and visualize respective T cell populations [134]. There is concrete evidence that CD4^{+} and CD8^{+} lymphocytes increasingly infiltrating the tumor microenvironment connote a response to immunotherapy and a favorable prognosis [135].

Tumor cells can upregulate the expression of PD-L1, which interacts with PD-1 on T cells [136]. The PD-1/PD-L1 interaction plays a major role in the inhibition of T cell activity [135, 136]. Preliminary clinical studies [68, 137] showed that [89]Zr-Df-nivolumab PET was a safe and feasible method to map the localization of PD-1-expressing T cells and to assess their PD-1 expression *in vivo*; a correlation between [89]Zr-Df-nivolumab uptake intensity and the number of PD-1-expressing lymphocytes in biopsied tumor was observed. Higashikawa et al. developed a CTLA-4-targeting PET probe (^{64}Cu-DOTA-anti-CTLA-4 mAb) to examine the expression of CLTA-4 in CT26 tumor-bearing mice [138]. They found that tumor-infiltrating T cells were responsible for the high CTLA-4 expression.

A recent investigation from Xiao et al. identified Inducible T-cell COStimulator (ICOS or CD278) as a costimulatory molecule upregulated during T cell activation [47]. They designed an ICOS-targeting tool ([89]Zr-DFO-ICOS mAb PET) for visualizing the activation of T cells and prediction of therapeutic response in the Lewis lung cancer model. Based on this work, [89]Zr-DFO-ICOS mAb PET/CT has recently been used to visualize CAR-T cell activation. Significantly higher PET signal was detected in the bone marrow of mice with systemic B-cell lymphoma mice treated with CD19 CAR-T cells, which reflected their distribution and activation [139].

Metabolism-based T cell imaging

When activated, T cells are metabolically programmed to switching on additional metabolic processes and upregulate substrate inflow, which allows them to develop full effector phenotypes, and survive and function in peripheral tissues [46]. Targeting these metabolic pathways can help to distinguish between activated and non-activated T cells, as well as to assess ensuing immune response at early time point.

Several tracers have been developed as substrates for enzymes, such as deoxycytidine kinase (dCK) and deoxyguanosine kinase (dGK), which are rate-limiting enzymes in the deoxyribonucleoside salvage pathway [46]. ^{18}F-CFA (^{18}F-clofarabine) is a nucleotide purine analogue metabolized *via* dCK, which has preferential *in vivo* distribution in hematopoietic bone marrow and secondary lymphoid organs [140]. ^{18}F-AraG (^{18}F-Arabinosyl guanine), another PET probe that targets specific metabolic pathways of T cells, accumulates in activated T cells, mainly *via* the dGK pathway [141]. ^{18}F-AraG PET imaging of a murine acute graft-*versus*-host-disease (aGVHD) model has been shown to visualize the activation of donor T cells in secondary lymphoid organs prior to the appearance of aGVHD symptoms [142]. Other PET tracers that target metabolic pathways, such as ^{18}F labeled fluorodeoxyglucose (FDG) and fluorothymidine (FLT), can also potentially monitor multiple cell types involved in innate and adaptive immunity and measure cell function [143].

In summary, endogenous cell imaging has shown the feasibility of direct assessment of the

presence, localization, numbers, activation and functional status of specific cell populations such as CTLs *in vivo* during immunotherapy [35, 46, 141], which can provide key information about the role of CAR-T cells in cellular immunotherapy, and promote the understanding and improvement of CAR-T immunotherapy. Nevertheless, the chief drawback to the application of endogenous cell imaging methods for CAR-T visualization is the nonspecific uptake of probe by the endogenous T cells, which cannot be distinguished from infused CAR-T cells.

Current challenges and strategy choice

The preclinical studies [48, 54] and clinical trials [64, 77] discussed above have already answered some of the questions about CAR-T monitoring raised in the Introduction. Both direct imaging and indirect imaging can provide spatial information on the transferred cells. This is beneficial not only to observe the trafficking, homing, expansion, contraction, and retention of cells through PET/SPECT signal detection and quantification, but also to determine whether there is nonspecific uptake in normal tissues, which is crucial for assessing the off-tumor/on-target toxicity. PET and SPECT images, especially fusion images integrated with CT or MRI, can provide tomographic and anatomic information. This is of great help in mapping the accurate spatial distribution of CAR-T cells in multiple dimensions, and in assessing whether CAR-T cells are infiltrating tumors. In addition, the activation and functional status of T cells can be monitored through metabolic pathway-/cell marker-targeting imaging [137, 139]. Notably, judging whether the expansion or contraction of cells matches the change in tumor burden can indirectly reflect ineffective proliferation (T cells continue to proliferate, but the tumor is not controlled) or effective killing (the tumor shrinks after T cell expansion) [109].

The choice of imaging strategy depends on several key aspects, including imaging technology, modality, and radionuclide. Compared with direct labeling and endogenous T cell imaging, reporter-based imaging is a more promising technique for visualizing and monitoring of CAR-T cells due to the advantages mentioned above. Nevertheless, two issues require scrutiny: immunogenicity and inherent expression of reporter genes. Focusing on identification of new human reporter genes may address the former issue. Choosing an appropriate reporter gene system for a specific clinical setting can help to weaken the influence caused by endogenous expression of reporter gene. For example, although hNIS is highly expressed in the thyroid, salivary glands and stomach [89-91], we can still apply hNIS-based reporter imaging for trafficking the CAR-T cells in other organs without hNIS expression, which provides a low background so that CAR-T cells can be detected easily.

The choice of imaging modalities (PET or SPECT) is also of great significance for the choice of imaging instrument and corresponding nuclides. The spatial resolution of PET (6–10 mm) is slightly better than that of SPECT (7–15 mm), and the sensitivity is an order of magnitude higher than that of SPECT (10^{-11}–^{12} *versus* 10^{-10}–^{11} mol/L probe) [29]. In terms of radionuclides, ^{18}F and ^{68}Ga would be good choices due to their accessibility. They have relative shorter half-lives, which are practical for human PET imaging. ^{89}Zr and ^{111}In have longer half-lives, which is beneficial for direct labeling methods to broaden their imaging time window [48, 52]. However, reporter gene imaging can be performed repeatedly, and patients will not need frequent repeat imaging with a very short interval. Therefore, long half-life radionuclides may increase the radiation dose, and not add value for trafficking T cells.

The choice of precursor (or nuclide carrier) also has a major impact on imaging. Although nanomaterials are highly modifiable and have diversified functions, their potential toxicity is always a thorny issue for researchers. Therefore, human imaging is mainly based on small molecules. Since previous data have confirmed their safety and feasibility, the small molecule probes that have been used in clinical practice (such as ^{68}Ga-DOTATOC and ^{18}F-DCFPyL) will be more widely used. If researchers design a new imaging probe, some important characteristics should be taken into consideration, such as multiple radionuclide compatibility, fast clearance *in vivo*, low cytotoxicity, and a high target-to-background ratio.

Conclusions and Perspective

A variety of strategies have been developed to enhance the therapeutic effect of CAR-T in solid tumors, such as potentiating the tumor killing [144, 145], improving the migration capacity [146, 147], infiltration ability [148, 149], and safety [150], as well as combining with radiotherapy [151, 152] or immune checkpoint blocking treatment [153, 154]. However, whichever strategies are employed, CAR-T cell monitoring is required for in-depth understanding of the therapeutic mechanism and to provide the basis for optimization. Noninvasive imaging, especially the reporter gene imaging approach, provides a tool for continuous and dynamic assessment of the distribution, migration, and function of human CAR-T cells. This field is gradually maturing and exhibits strong clinical translation potential. For

certain clinical scenarios, the development of novel reporter gene systems or the rational selection of existing reporter/probe pairs is a key step to addressing the issues that arise during the continuous exploration and optimization of CAR-T therapy in solid tumors.

Abbreviations

ACT: adoptive cell therapy; CAR: chimeric antigen receptor; IFN: interfron; IL-2: interleukin 2; CXCR-2: C-X-C chemokine receptor type 2; CT: computed tomography; MRI: magnetic resonance imaging; OI: optical imaging; BLI: bioluminescence imaging; FLI: fluorescence imaging; PET: positron emission tomography; SPECT: single photon emission computed tomography; SCID: severe combined immunodeficiency; IL13Rα2: interleukin-13 receptor α2; PSCA: prostate stem cell antigen; NSG: nonobese diabetic severe combined immunodeficient; GNP: gold nanoparticle; DOTA: 1,4,7,10-tetraazacyclo-dodecane-1,4,7,10-tetraacetic acid; PEG: polyethylene-glycol; DNA: Deoxyribonucleic acid; HSV-1 tk: herpes simplex virus 1 thymidine kinase; FIAU: 2-fluoro-2-deoxy-1-β-D-arabinofuranosyl-5-iodouracil; FHBG: 9-(4-fluoro-3-hydroxymethylbutyl)guanine; FEAU: 2-deoxy-2-fluoro-5-ethyl-β-D-arabinofuranosyl-uracil; FHPG: 9-(3-fluoro-1-hydroxy-2-propoxymethyl) guanine; CTL: cytotoxic T lymphocyte; TCR: T-cell receptor; NFAT: nuclear factor of activated T cells; IL-13: interleukin 13; SUVmean: mean standard uptake value; eDHFR: *E. coli* dihydrofolate reductase; TMP: fluoropropyl-trimethoprim; p.t: post T cells infusion; hNIS: human sodium-iodine symporter; PSMA: prostate-specific membrane antigen; PD-L1: programmed cell death protein ligand 1; SSTR: somatostatin receptor; DOTATATE: 1,4,7,10-tetra-azacyclododecane-$N^I,N^{II},N^{III},N^{IIII}$-tetraacetic acid-d-Phe1-Tyr3-octreotate; DOTATOC: 1,4,7,10-tetraaza-cyclododecane-$N^I,N^{II},N^{III},N^{IIII}$-tetraacetic acid (D)-Phe1-thy3-octreotide; ICAM-1: intercellular adhesion molecule-1; ^{18}F-DCFPyL: 2-(3-{1-carboxy-5-[(6-^{18}F-fluoro-pyridine-3-carbonyl)-amino]-pentyl}-ureido)-pentanedioic acid; eGFP: enhanced green fluorescent protein; hNET: human norepinephrine transporter; MIBG: metaiodobenzylguanidine; hdCKDM: human deoxycytidine kinase double mutant; DAbR1: DOTA antibody reporter 1; AABD: lanthanoid-(S)-2-(4-acrylamidobenzyl)-DOTA; MIP: maximum intensity projection PD-1 programmed cell death protein 1; CTLA-4: cytotoxic T-lymphocyte-associated protein 4; scFv: single chain variable fragment; ICOS: inducible T-cell COStimulator; dCK: deoxycytidine kinase; dGK: deoxyguanosine kinase; aGVHD: acute graft-versus-host-disease; FDG: fluorodeoxyglucose; FLT: fluorothymidine.

Competing Interests

The authors have declared that no competing interest exists.

References

1. Hoos A. Development of immuno-oncology drugs - from CTLA4 to PD1 to the next generations. Nat Rev Drug Discov. 2016; 15: 235-47.
2. Morgan MA, Schambach A. Engineering CAR-T Cells for Improved Function against Solid Tumors. Front Immunol. 2018; 9: 2493.
3. Geyer MB, Brentjens RJ. Review: Current clinical applications of chimeric antigen receptor (CAR) modified T cells. Cytotherapy. 2016; 18: 1393-409.
4. Turtle CJ, Riddell SR, Maloney DG. CD19-Targeted chimeric antigen receptor-modified T-cell immunotherapy for B-cell malignancies. Clin Pharmacol Ther. 2016; 100: 252-8.
5. Grupp SA, Kalos M, Barrett D, Aplenc R, Porter DL, Rheingold SR, et al. Chimeric antigen receptor-modified T cells for acute lymphoid leukemia. N Engl J Med. 2013; 368: 1509-18.
6. Porter DL, Levine BL, Kalos M, Bagg A, June CH. Chimeric antigen receptor-modified T cells in chronic lymphoid leukemia. N Engl J Med. 2011; 365: 725-33.
7. Neelapu SS, Locke FL, Bartlett NL, Lekakis LJ, Miklos DB, Jacobson CA, et al. Axicabtagene Ciloleucel CAR T-Cell Therapy in Refractory Large B-Cell Lymphoma. N Engl J Med. 2017; 377: 2531-44.
8. Sadelain M. CAR therapy: the CD19 paradigm. J Clin Invest. 2015; 125: 3392-400.
9. Ruella M, Barrett DM, Kenderian SS, Shestova O, Hofmann TJ, Perazzelli J, et al. Dual CD19 and CD123 targeting prevents antigen-loss relapses after CD19-directed immunotherapies. J Clin Invest. 2016; 126: 3814-26.
10. Rodriguez-Garcia A, Palazon A, Noguera-Ortega E, Powell DJ, Jr., Guedan S. CAR-T Cells Hit the Tumor Microenvironment: Strategies to Overcome Tumor Escape. Front Immunol. 2020; 11: 1109.
11. D'Aloia MM, Zizzari IG, Sacchetti B, Pierelli L, Alimandi M. CAR-T cells: the long and winding road to solid tumors. Cell Death Dis. 2018; 9: 282.
12. Xu J, Wang Y, Shi J, Liu J, Li Q, Chen L. Combination therapy: A feasibility strategy for CAR-T cell therapy in the treatment of solid tumors. Oncol Lett. 2018; 16: 2063-70.
13. Jo Y, Auid O, Ali LA, Auid- Orcid X, Shim JA, Lee BH, et al. Innovative CAR-T Cell Therapy for Solid Tumor; Current Duel between CAR-T Spear and Tumor Shield. Cancers. 2020; 12.
14. Peng W, Ye Y, Rabinovich BA, Liu C, Lou Y, Zhang M, et al. Transduction of tumor-specific T cells with CXCR2 chemokine receptor improves migration to tumor and antitumor immune responses. Clin Cancer Res. 2010; 16: 5458-68.
15. Caruana I, Savoldo B, Hoyos V, Weber G, Liu H, Kim ES, et al. Heparanase promotes tumor infiltration and antitumor activity of CAR-redirected T lymphocytes. Nat Med. 2015; 21: 524-9.
16. Khalil DN, Smith EL, Brentjens RJ, Wolchok JD. The future of cancer treatment: immunomodulation, CARs and combination immunotherapy. Nat Rev Clin Oncol. 2016; 13: 273-90.
17. Klaver Y, Kunert A, Sleijfer S, Debets R, Lamers CH. Adoptive T-cell therapy: a need for standard immune monitoring. Immunotherapy. 2015; 7: 513-33.
18. Li H, Zhao Y. Increasing the safety and efficacy of chimeric antigen receptor T cell therapy. Protein Cell. 2017; 8: 573-89.
19. Lee DW, Gardner R, Porter DL, Louis CU, Ahmed N, Jensen M, et al. Current concepts in the diagnosis and management of cytokine release syndrome. Blood. 2014; 124: 188-95.
20. Neelapu SS, Tummala S, Kebriaei P, Wierda W, Gutierrez C, Locke FL, et al. Chimeric antigen receptor T-cell therapy - assessment and management of toxicities. Nat Rev Clin Oncol. 2018; 15: 47-62.
21. Feng K, Guo Y, Dai H, Wang Y, Li X, Jia H, et al. Chimeric antigen receptor-modified T cells for the immunotherapy of patients with EGFR-expressing advanced relapsed/refractory non-small cell lung cancer. Sci China Life Sci. 2016; 59: 468-79.

22. Zhang C, Wang Z, Yang Z, Wang M, Li S, Li Y, et al. Phase I Escalating-Dose Trial of CAR-T Therapy Targeting CEA(+) Metastatic Colorectal Cancers. Mol Ther. 2017; 25: 1248-58.

23. Weissleder R, Mahmood U. Molecular imaging. Radiology. 2001; 219: 316-33.

24. Henriquez NV, van Overveld PG, Que I, Buijs JT, Bachelier R, Kaijzel EL, et al. Advances in optical imaging and novel model systems for cancer metastasis research. Clin Exp Metastasis. 2007; 24: 699-705.

25. Tian J, Bai J, Yan XP, Bao S, Li Y, Liang W, et al. Multimodality molecular imaging. IEEE Eng Med Biol Mag 2008; 27: 48-57.

26. Xing Y, Zhao J, Conti PS, Chen K. Radiolabeled nanoparticles for multimodality tumor imaging. Theranostics. 2014; 4: 290-306.

27. Niers JM, Chen JW, Lewandrowski G, Kerami M, Garanger E, Wojtkiewicz G, et al. Single reporter for targeted multimodal *in vivo* imaging. J Am Chem Soc. 2012; 134: 5149-56.

28. Reader AJ, Zweit J. Developments in whole-body molecular imaging of live subjects. Trends Pharmacol Sci. 2001; 22: 604-7.

29. Nguyen PK, Lan F, Wang Y, Wu JC. Imaging: guiding the clinical translation of cardiac stem cell therapy. Circ Res. 2011; 109: 962-79.

30. Zhang Y, Yang Y, Cai W. Multimodality Imaging of Integrin alpha(v)beta(3) Expression. Theranostics. 2011; 1: 135-48.

31. Wu MR, Liu HM, Lu CW, Shen WH, Lin IJ, Liao LW, et al. Organic anion-transporting polypeptide 1B3 as a dual reporter gene for fluorescence and magnetic resonance imaging. FASEB J . 2018; 32: 1705-15.

32. Wagenaar DJ, Kapusta M, Li J, Patt BE. Rationale for the combination of nuclear medicine with magnetic resonance for pre-clinical imaging. Technol Cancer Res Treat. 2006; 5: 343-50.

33. Bailey DL, Willowson KP. An evidence-based review of quantitative SPECT imaging and potential clinical applications. J Nucl Med. 2013; 54: 83-9.

34. Basu S, Kwee TC, Surti S, Akin EA, Yoo D, Alavi A. Fundamentals of PET and PET/CT imaging. Ann N Y Acad Sci. 2011; 1228: 1-18.

35. Wei W, Jiang D, Ehlerding EB, Luo Q, Cai W. Noninvasive PET Imaging of T cells. Trends Cancer. 2018; 4: 359-73.

36. Perez-Medina C, Teunissen AJP, Kluza E, Mulder WJM, van der Meel R. Nuclear imaging approaches facilitating nanomedicine translation. Adv Drug Deliv Rev. 2020.

37. McCarthy CE, White JM, Viola NT, Gibson HM. *In vivo* Imaging Technologies to Monitor the Immune System. Front Immunol. 2020; 11: 1067.

38. Kircher MF, Gambhir SS, Grimm J. Noninvasive cell-tracking methods. Nat Rev Clin Oncol. 2011; 8: 677-88.

39. Zhou R, Thomas DH, Qiao H, Bal HS, Choi SR, Alavi A, et al. *In vivo* detection of stem cells grafted in infarcted rat myocardium. J Nucl Med. 2005; 46: 816-22.

40. Pittet MJ, Grimm J, Berger CR, Tamura T, Wojtkiewicz G, Nahrendorf M, et al. *In vivo* imaging of T cell delivery to tumors after adoptive transfer therapy. Proc Natl Acad Sci U S A. 2007; 104: 12457-61.

41. Blasberg RG, Gelovani-Tjuvajev J. *In vivo* molecular-genetic imaging. J Cell Biochem Suppl. 2002; 39: 172-83.

42. Kang JH, Chung JK. Molecular-genetic imaging based on reporter gene expression. J Nucl Med. 2008; 49 Suppl 2: 164S-79S.

43. Dobrenkov K, Olszewska M, Likar Y, Shenker L, Gunset G, Cai S, et al. Monitoring the efficacy of adoptively transferred prostate cancer-targeted human T lymphocytes with PET and bioluminescence imaging. J Nucl Med. 2008; 49: 1162-70.

44. Gambhir SS, Herschman HR, Cherry SR, Barrio JR, Satyamurthy N, Toyokuni T, et al. Imaging transgene expression with radionuclide imaging technologies. Neoplasia. 2000; 2: 118-38.

45. Yaghoubi SS, Gambhir SS. PET imaging of herpes simplex virus type 1 thymidine kinase (HSV1-tk) or mutant HSV1-sr39tk reporter gene expression in mice and humans using [18F]FHBG. Nat Protoc. 2006; 1: 3069-75.

46. Krekorian M, Fruhwirth GO, Srinivas M, Figdor CG, Heskamp S, Witney TH, et al. Imaging of T-cells and their responses during anti-cancer immunotherapy. Theranostics. 2019; 9: 7924-47.

47. Xiao Z, Mayer AT, Nobashi TW, Gambhir SS. ICOS Is an Indicator of T-cell-Mediated Response to Cancer Immunotherapy. Cancer Res. 2020; 80: 3023-32.

48. Parente-Pereira AC, Burnet J, Ellison D, Foster J, Davies DM, van der Stegen S, et al. Trafficking of CAR-engineered human T cells following regional or systemic adoptive transfer in SCID beige mice. J Clin Immunol. 2011; 31: 710-8.

49. Weist MR, Starr R, Aguilar B, Chea J, Miles JK, Poku E, et al. PET of Adoptively Transferred Chimeric Antigen Receptor T Cells with (89)Zr-Oxine. J Nucl Med. 2018; 59: 1531-7.

50. Bhatnagar P, Li Z, Choi Y, Guo J, Li F, Lee DY, et al. Imaging of genetically engineered T cells by PET using gold nanoparticles complexed to Copper-64. Integr Biol (Camb) . 2013; 5: 231-8.

51. Man F, Lim L, Volpe A, Gabizon A, Shmeeda H, Draper B, et al. *In vivo* PET Tracking of (89)Zr-Labeled Vgamma9Vdelta2 T Cells to Mouse Xenograft Breast Tumors Activated with Liposomal Alendronate. Mol Ther. 2019; 27: 219-29.

52. Charoenphun P, Meszaros LK, Chuamsaamarkkee K, Sharif-Paghaleh E, Ballinger JR, Ferris TJ, et al. [(89)Zr]oxinate4 for long-term *in vivo* cell tracking by positron emission tomography. Eur J Nucl Med Mol Imaging. 2015; 42: 278-87.

53. Sato N, Wu H, Asiedu KO, Szajek LP, Griffiths GL, Choyke PL. (89)Zr-Oxine Complex PET Cell Imaging in Monitoring Cell-based Therapies. Radiology. 2015; 275: 490-500.

54. Oh E, Delehanty JB, Sapsford KE, Susumu K, Goswami R, Blanco-Canosa JB, et al. Cellular uptake and fate of PEGylated gold nanoparticles is dependent on both cell-penetration peptides and particle size. ACS nano. 2011; 5: 6434-48.

55. Guo Y, Feng K, Liu Y, Wu Z, Dai H, Yang Q, et al. Phase I Study of Chimeric Antigen Receptor-Modified T Cells in Patients with EGFR-Positive Advanced Biliary Tract Cancers. Clin Cancer Res. 2018; 24: 1277-86.

56. Wang Y, Chen M, Wu Z, Tong C, Dai H, Guo Y, et al. CD133-directed CAR T cells for advanced metastasis malignancies: A phase I trial. Oncoimmunology. 2018; 7: e1440169.

57. Massoud TF, Singh A, Gambhir SS. Noninvasive molecular neuroimaging using reporter genes: part I, principles revisited. AJNR Am J Neuroradiol. 2008; 29: 229-34.

58. Emami-Shahri N, Foster J, Kashani R, Gazinska P, Cook C, Sosabowski J, et al. Clinically compliant spatial and temporal imaging of chimeric antigen receptor T-cells. Nat Commun. 2018; 9: 1081.

59. Minn I, Auid- Orcid X, Huss DJ, Ahn HH, Chinn TM, Park A, et al. Imaging CAR T cell therapy with PSMA-targeted positron emission tomography. Sci Adv. 2019; 5: eaaw5096.

60. Nair-Gill ED, Shu CJ, Radu CG, Witte ON. Non-invasive imaging of adaptive immunity using positron emission tomography. Immunol Rev. 2008; 221: 214-28.

61. Koya RC, Mok S, Comin-Anduix B, Chodon T, Radu CG, Nishimura MI, et al. Kinetic phases of distribution and tumor targeting by T cell receptor engineered lymphocytes inducing robust antitumor responses. Proc Natl Acad Sci U S A. 2010; 107: 14286-91.

62. Moroz MA, Zhang H, Lee J, Moroz E, Zurita J, Shenker L, et al. Comparative Analysis of T Cell Imaging with Human Nuclear Reporter Genes. J Nucl Med. 2015; 56: 1055-60.

63. Min JJ, Gambhir SS. Molecular imaging of PET reporter gene expression. Handb Exp Pharmacol. 2008; p: 277-303.

64. Yaghoubi SS, Jensen MC, Satyamurthy N, Budhiraja S, Paik D, Czernin J, et al. Noninvasive detection of therapeutic cytolytic T cells with 18F-FHBG PET in a patient with glioma. Nat Clin Pract Oncol. 2009; 6: 53-8.

65. Brust P, Haubner R, Friedrich A, Scheunemann M, Anton M, Koufaki ON, et al. Comparison of [18F]FHPG and [124/125I]FIAU for imaging herpes simplex virus type 1 thymidine kinase gene expression. Eur J Nucl Med. 2001; 28: 721-9.

66. Soghomonyan S, Hajitou A, Rangel R, Trepel M, Pasqualini R, Arap W, et al. Molecular PET imaging of HSV1-tk reporter gene expression using [18F]FEAU. Nat Protoc. 2007; 2: 416-23.

67. Tjuvajev JG, Doubrovin M, Akhurst T, Cai S, Balatoni J, Alauddin MM, et al. Comparison of radiolabeled nucleoside probes (FIAU, FHBG, and FHPG) for PET imaging of HSV1-tk gene expression. J Nucl Med. 2002; 43: 1072-83.

68. Min JJ, Iyer M, Gambhir SS. Comparison of [18F]FHBG and [14C]FIAU for imaging of HSV1-tk reporter gene expression: adenoviral infection vs stable transfection. Eur J Nucl Med Mol Imaging. 2003; 30: 1547-60.

69. Koehne G, Doubrovin M, Doubrovina E, Zanzonico P, Gallardo HF, Ivanova A, et al. Serial *in vivo* imaging of the targeted migration of human HSV-TK-transduced antigen-specific lymphocytes. Nat Biotechnol. 2003; 21: 405-13.

70. Thunemann M, Schorg BF, Feil S, Lin Y, Voelkl J, Golla M, et al. Cre/lox-assisted non-invasive *in vivo* tracking of specific cell populations by positron emission tomography. Nat Commun. 2017; 8: 444.

71. Salabert AS, Vaysse L, Beaurain M, Alonso M, Arribarat G, Lotterie JA, et al. Imaging grafted cells with [18F]FHBG using an optimized HSV1-TK mammalian expression vector in a brain injury rodent model. PLoS One. 2017; 12: e0184630.

72. Pei Z, Lan X, Cheng Z, Qin C, Xia X, Yuan H, et al. Multimodality molecular imaging to monitor transplanted stem cells for the treatment of ischemic heart disease. PLoS One. 2014; 9: e90543.

73. Dotti G, Tian M, Savoldo B, Najjar A, Cooper LJ, Jackson J, et al. Repetitive noninvasive monitoring of HSV1-tk-expressing T cells intravenously infused into nonhuman primates using positron emission tomography and computed tomography with 18F-FEAU. Mol Imaging. 2009; 8: 230-7.

74. Ponomarev V, Doubrovin M, Lyddane C, Beresten T, Balatoni J, Bornman W, et al. Imaging TCR-dependent NFAT-mediated T-cell activation with positron emission tomography *in vivo*. Neoplasia. 2001; 3: 480-8.

75. Yaghoubi S, Barrio JR, Dahlbom M, Iyer M, Namavari M, Satyamurthy N, et al. Human pharmacokinetic and dosimetry studies of [(18)F]FHBG: a reporter probe for imaging herpes simplex virus type-1 thymidine kinase reporter gene expression. J Nucl Med. 2001; 42: 1225-34.

76. Yaghoubi SS, Gambhir SS. PET imaging of herpes simplex virus type 1 thymidine kinase (HSV1-tk) or mutant HSV1-sr39tk reporter gene expression in mice and humans using [18F]FHBG. Nat Protoc. 2006; 1: 3069-75.

77. Keu KV, Witney TH, Yaghoubi S, Rosenberg J, Kurien A, Magnusson R, et al. Reporter gene imaging of targeted T cell immunotherapy in recurrent glioma. Sci Transl Med. 2017; 9.

78. Yaghoubi SS, Campbell DO, Radu CG, Czernin J. Positron emission tomography reporter genes and reporter probes: gene and cell therapy applications. Theranostics. 2012; 2: 374-91.

79. Serganova I, Ponomarev V, Blasberg R. Human reporter genes: potential use in clinical studies. Nucl Med Biol. 2007; 34: 791-807.

80. Sellmyer MA, Lee I, Hou C, Lieberman BP, Zeng C, Mankoff DA, et al. Quantitative PET Reporter Gene Imaging with [(11)C]Trimethoprim. Mol Ther. 2017; 25: 120-6.

81. Sellmyer MA, Auid O, Lee I, Hou C, Weng CC, Li S, et al. Bacterial infection imaging with [(18)F]fluoropropyl-trimethoprim. Proc Natl Acad Sci U S A. 2017; 114: 8372-7.

82. Kremers P, Duvivier J, Heusghem C. Pharmacokinetic studies of co-trimoxazole in man after single and repeated doses. J Clin Pharmacol. 1974; 14: 112-7.

83. Ingebrigtsen K, Skoglund LA, Nafstad I. A study on melanin affinity of 14C-trimethoprim in male Mol:WIST and Mol:PVG rats. Z Versuchstierkd. 1990; 33: 73-5.

84. Sellmyer MA, Richman SA, Lohith K, Hou C, Weng CC, Mach RH, et al. Imaging CAR T Cell Trafficking with eDHFR as a PET Reporter Gene. Mol Ther. 2020; 28: 42-51.

85. Liu CT, Hanoian P, French JB, Pringle TH, Hammes-Schiffer S, Benkovic SJ. Functional significance of evolving protein sequence in dihydrofolate reductase from bacteria to humans. Proc Natl Acad Sci U S A. 2013; 110: 10159-64.

86. Campbell DO, Yaghoubi SS, Su Y, Lee JT, Auerbach MS, Herschman H, et al. Structure-guided engineering of human thymidine kinase 2 as a positron emission tomography reporter gene for enhanced phosphorylation of non-natural thymidine analog reporter probe. J Biol Chem. 2012; 287: 446-54.

87. Nicola JP, Basquin C, Portulano C, Reyna-Neyra A, Paroder M, Carrasco N. The Na+/I- symporter mediates active iodide uptake in the intestine. Am J Physiol Cell Physiol. 2009; 296: C654-62.

88. Portulano C, Paroder-Belenitsky M, Carrasco N. The Na+/I- symporter (NIS): mechanism and medical impact. Endocr Rev. 2014; 35: 106-49.

89. Spitzweg C, Joba W, Eisenmenger W, Heufelder AE. Analysis of human sodium iodide symporter gene expression in extrathyroidal tissues and cloning of its complementary deoxyribonucleic acids from salivary gland, mammary gland, and gastric mucosa. J Clin Endocrinol Metab. 1998; 83: 1746-51.

90. Dadachova E, Carrasco N. The Na/I symporter (NIS): imaging and therapeutic applications. Semin Nucl Med. 2004; 34: 23-31.

91. Ravera S, Reyna-Neyra A, Ferrandino G, Amzel LM, Carrasco N. The Sodium/Iodide Symporter (NIS): Molecular Physiology and Preclinical and Clinical Applications. Annu Rev Physiol. 2017; 79: 261-89.

92. Penheiter AR, Russell SJ, Carlson SK. The sodium iodide symporter (NIS) as an imaging reporter for gene, viral, and cell-based therapies. Curr Gene Ther. 2012; 12: 33-47.

93. Chung JK. Sodium iodide symporter: its role in nuclear medicine. J Nucl Med. 2002; 43: 1188-200.

94. Lee HW, Jeon YH, Hwang MH, Kim JE, Park TI, Ha JH, et al. Dual reporter gene imaging for tracking macrophage migration using the human sodium iodide symporter and an enhanced firefly luciferase in a murine inflammation model. Mol Imaging Biol. 2013; 15: 703-12.

95. Lee HW, Yoon SY, Singh TD, Choi YJ, Lee HJ, Park JY, et al. Tracking of dendritic cell migration into lymph nodes using molecular imaging with sodium iodide symporter and enhanced firefly luciferase genes. Sci Rep. 2015; 5: 9865.

96. Seo JH, Jeon YH, Lee YJ, Yoon GS, Won DI, Ha JH, et al. Trafficking macrophage migration using reporter gene imaging with human sodium iodide symporter in animal models of inflammation. J Nucl Med. 2010; 51: 1637-43.

97. Hickey RD, Mao SA, Glorioso J, Elgilani F, Amiot B, Chen H, et al. Curative *ex vivo* liver-directed gene therapy in a pig model of hereditary tyrosinemia type 1. Sci Transl Med. 2016; 8: 349ra99.

98. Holvoet B, Quattrocelli M, Belderbos S, Pollaris L, Wolfs E, Gheysens O, et al. Sodium Iodide Symporter PET and BLI Noninvasively Reveal Mesoangioblast Survival in Dystrophic Mice. Stem cell reports. 2015; 5: 1183-95.

99. Lee AR, Woo SK, Kang SK, Lee SY, Lee MY, Park NW, et al. Adenovirus-mediated expression of human sodium-iodide symporter gene permits *in vivo* tracking of adipose tissue-derived stem cells in a canine myocardial infarction model. Nucl Med Biol. 2015; 42: 621-9.

100. Diocou S, Volpe A, Jauregui-Osoro M, Boudjemeline M, Chuamsaamarkkee K, Man F, et al. [(18)F]tetrafluoroborate-PET/CT enables sensitive tumor and metastasis *in vivo* imaging in a sodium iodide symporter-expressing tumor model. Sci Rep. 2017; 7: 946.

101. Fruhwirth GO, Diocou S, Blower PJ, Ng T, Mullen GE. A whole-body dual-modality radionuclide optical strategy for preclinical imaging of metastasis and heterogeneous treatment response in different microenvironments. J Nucl Med. 2014; 55: 686-94.

102. Volpe A, Man F, Lim L, Khoshnevisan A, Blower J, Blower PJ, et al. Radionuclide-fluorescence Reporter Gene Imaging to Track Tumor Progression in Rodent Tumor Models. J Vis Exp. 2018.

103. Dwyer RM, Ryan J, Havelin RJ, Morris JC, Miller BW, Liu Z, et al. Mesenchymal Stem Cell-mediated delivery of the sodium iodide symporter supports radionuclide imaging and treatment of breast cancer. Stem cells. 2011; 29: 1149-57.

104. Shu CJ, Radu CG, Shelly SM, Vo DD, Prins R, Ribas A, et al. Quantitative PET reporter gene imaging of CD8+ T cells specific for a melanoma-expressed self-antigen. Int Immunol. 2009; 21: 155-65.

105. Volpe A, Lang C, Lim L, Man F, Kurtys E, Ashmore-Harris C, et al. Spatiotemporal PET Imaging Reveals Differences in CAR-T Tumor Retention in Triple-Negative Breast Cancer Models. Mol Ther. 2020; 28: 2271-85.

106. Cuevas-Ramos D, Fleseriu M. Somatostatin receptor ligands and resistance to treatment in pituitary adenomas. J Mol Endocrinol. 2014; 52: R223-40.

107. Yamada Y, Post SR, Wang K, Tager HS, Bell GI, Seino S. Cloning and functional characterization of a family of human and mouse somatostatin receptors expressed in brain, gastrointestinal tract, and kidney. Proc Natl Acad Sci U S A. 1992; 89: 251-5.

108. Xu C, Auid O, Zhang H. Somatostatin receptor based imaging and radionuclide therapy. Biomed Res Int. 2015; 2015: 917968.

109. Vedvyas Y, Shevlin E, Zaman M, Min IM, Amor-Coarasa A, Park S, et al. Longitudinal PET imaging demonstrates biphasic CAR T cell responses in survivors. JCI insight. 2016; 1: e90064.

110. Elliott DE, Li J, Blum AM, Metwali A, Patel YC, Weinstock JV. SSTR2A is the dominant somatostatin receptor subtype expressed by inflammatory cells, is widely expressed and directly regulates T cell IFN-gamma release. Eur J Immunol. 1999; 29: 2454-63.

111. Ashmore-Harris C, Iafrate M, Saleem A, Fruhwirth GO. Non-invasive Reporter Gene Imaging of Cell Therapies, including T Cells and Stem Cells. Mol Ther. 2020; 28: 1392-416.

112. Cescato R, Schulz S, Waser B, Eltschinger V, Rivier JE, Wester HJ, et al. Internalization of sst2, sst3, and sst5 receptors: effects of somatostatin agonists and antagonists. J Nucl Med. 2006; 47: 502-11.

113. Sweat SD, Pacelli A, Murphy GP, Bostwick DG. Prostate-specific membrane antigen expression is greatest in prostate adenocarcinoma and lymph node metastases. Urology. 1998; 52: 637-40.

114. Silver DA, Pellicer I, Fair WR, Heston WD, Cordon-Cardo C. Prostate-specific membrane antigen expression in normal and malignant human tissues. Clin Cancer Res. 1997; 3: 81-5.

115. Castanares MA, Mukherjee A, Chowdhury WH, Liu M, Chen Y, Mease RC, et al. Evaluation of prostate-specific membrane antigen as an imaging reporter. J Nucl Med. 2014; 55: 805-11.

116. Guo H, Kommidi H, Vedvyas Y, McCloskey JE, Zhang W, Auid O, et al. A Fluorescent, [(18)F]-Positron-Emitting Agent for Imaging Prostate-Specific Membrane Antigen Allows Genetic Reporting in Adoptively Transferred, Genetically Modified Cells. ACS Chem Biol. 2019; 14: 1449-59.

117. Rajasekaran SA, Anilkumar G, Oshima E, Bowie JU, Liu H, Heston W, et al. A novel cytoplasmic tail MXXXL motif mediates the internalization of prostate-specific membrane antigen. Mol Biol Cell. 2003; 14: 4835-45.

118. Doubrovin MM, Doubrovina ES, Zanzonico P, Sadelain M, Larson SM, O'Reilly RJ. *In vivo* imaging and quantitation of adoptively transferred human antigen-specific T cells transduced to express a human norepinephrine transporter gene. Cancer Res. 2007; 67: 11959-69.

119. Pacholczyk T, Blakely RD, Amara SG. Expression cloning of a cocaine- and antidepressant-sensitive human noradrenaline transporter. Nature. 1991; 350: 350-4.

120. Shulkin BL, Shapiro B, Tobes MC, Shen SW, Wieland DM, Meyers LJ, et al. Iodine-123-4-amino-3-iodobenzylguanidine, a new sympathoadrenal imaging agent: comparison with iodine-123 metaiodobenzylguanidine. J Nucl Med. 1986; 27: 1138-42.

121. Moroz MA, Serganova I, Zanzonico P, Ageyeva L, Beresten T, Dyomina E, et al. Imaging hNET reporter gene expression with 124I-MIBG. J Nucl Med. 2007; 48: 827-36.

122. Goodwin DA, Meares CF, Watanabe N, McTigue M, Chaovapong W, Ransone CM, et al. Pharmacokinetics of pretargeted monoclonal antibody 2D12.5 and 88Y-Janus-2-(p-nitrobenzyl)-1,4,7,10-tetraazacyclododecanetetraacetic acid (DOTA) in BALB/c mice with KHJJ mouse adenocarcinoma: a model for 90Y radioimmunotherapy. Cancer Res. 1994; 54: 5937-46.

123. Lubic SP, Goodwin DA, Meares CF, Song C, Osen M, Hays M. Biodistribution and dosimetry of pretargeted monoclonal antibody 2D12.5 and Y-Janus-DOTA in BALB/c mice with KHJJ mouse adenocarcinoma. J Nucl Med. 2001; 42: 670-8.

124. Corneillie TM, Whetstone PA, Lee KC, Wong JP, Meares CF. Converting weak binders into infinite binders. Bioconjug Chem. 2004; 15: 1389-91.

125. Krebs S, Ahad A, Carter LM, Eyquem J, Brand C, Bell M, et al. Antibody with Infinite Affinity for *In vivo* Tracking of Genetically Engineered Lymphocytes. J Nucl Med. 2018; 59: 1894-900.

126. Zanzonico P, Koehne G, Gallardo HF, Doubrovin M, Doubrovina E, Finn R, et al. [131I]FIAU labeling of genetically transduced, tumor-reactive lymphocytes: cell-level dosimetry and dose-dependent toxicity. Eur J Nucl Med Mol Imaging. 2006; 33: 988-97.

127. Li M, Wang Y, Liu M, Lan X. Multimodality reporter gene imaging: Construction strategies and application. Theranostics. 2018; 8: 2954-73.

128. Jahner D, Stuhlmann H, Stewart CL, Harbers K, Lohler J, Simon I, et al. De novo methylation and expression of retroviral genomes during mouse embryogenesis. Nature. 1982; 298: 623-8.

129. Ponomarev V. Advancing Immune and Cell-Based Therapies Through Imaging. Mol Imaging Biol. 2017; 19: 379-84.

130. Wu AM. Engineered antibodies for molecular imaging of cancer. Methods. 2014; 65: 139-47.

131. Tavare R, McCracken MN, Zettlitz KA, Salazar FB, Olafsen T, Witte ON, et al. Immuno-PET of Murine T Cell Reconstitution Postadoptive Stem Cell Transplantation Using Anti-CD4 and Anti-CD8 Cys-Diabodies. J Nucl Med. 2015; 56: 1258-64.

132. Larimer BM, Wehrenberg-Klee E, Caraballo A, Mahmood U. Quantitative CD3 PET Imaging Predicts Tumor Growth Response to Anti-CTLA-4 Therapy. J Nucl Med. 2016; 57: 1607-11.

133. Rashidian M, Ingram JR, Dougan M, Dongre A, Whang KA, LeGall C, et al. Predicting the response to CTLA-4 blockade by longitudinal noninvasive monitoring of CD8 T cells. J Exp Med. 2017; 214: 2243-55.
134. Seo JW, Tavare R, Mahakian LM, Silvestrini MT, Tam S, Ingham ES, et al. CD8(+) T-Cell Density Imaging with (64)Cu-Labeled Cys-Diabody Informs Immunotherapy Protocols. Clin Cancer Res. 2018; 24: 4976-87.
135. Freise AC, Zettlitz KA, Salazar FB, Lu X, Tavare R, Wu AM. ImmunoPET Imaging of Murine CD4(+) T Cells Using Anti-CD4 Cys-Diabody: Effects of Protein Dose on T Cell Function and Imaging. Mol Imaging Biol. 2017; 19: 599-609.
136. Sharpe AH, Pauken KE. The diverse functions of the PD1 inhibitory pathway. Nat Rev Immunol. 2018; 18: 153-67.
137. Niemeijer AN, Leung D, Huisman MC, Bahce I, Hoekstra OS, van Dongen G, et al. Whole body PD-1 and PD-L1 positron emission tomography in patients with non-small-cell lung cancer. Nat Commun. 2018; 9: 4664.
138. Higashikawa K, Yagi K, Watanabe K, Kamino S, Ueda M, Hiromura M, et al. 64Cu-DOTA-anti-CTLA-4 mAb enabled PET visualization of CTLA-4 on the T-cell infiltrating tumor tissues. PloS one. 2014; 9: e109866.
139. Simonetta F, Alam IS, Lohmeyer JK, Sahaf B, Good Z, Chen W, et al. Molecular Imaging of Chimeric Antigen Receptor T Cells by ICOS-ImmunoPET. Clin Cancer Res. 2020.
140. Barrio MJ, Spick C, Radu CG, Lassmann M, Eberlein U, Allen-Auerbach M, et al. Human Biodistribution and Radiation Dosimetry of (18)F-Clofarabine, a PET Probe Targeting the Deoxyribonucleoside Salvage Pathway. J Nucl Med. 2017; 58: 374-8.
141. Levi J, Lam T, Goth SR, Yaghoubi S, Bates J, Ren G, et al. Imaging of Activated T Cells as an Early Predictor of Immune Response to Anti-PD-1 Therapy. Cancer Res. 2019; 79: 3455-65.
142. Ronald JA, Kim BS, Gowrishankar G, Namavari M, Alam IS, D'Souza A, et al. A PET Imaging Strategy to Visualize Activated T Cells in Acute Graft-versus-Host Disease Elicited by Allogenic Hematopoietic Cell Transplant. Cancer Res. 2017; 77: 2893-902.
143. Laing RE, Nair-Gill E, Witte ON, Radu CG. Visualizing cancer and immune cell function with metabolic positron emission tomography. Curr Opin Genet Dev. 2010; 20: 100-5.
144. Li S, Siriwon N, Zhang X, Yang S, Jin T, He F, et al. Enhanced Cancer Immunotherapy by Chimeric Antigen Receptor-Modified T Cells Engineered to Secrete Checkpoint Inhibitors. Clin Cancer Res. 2017; 23: 6982-92.
145. Rafiq S, Yeku OO, Jackson HJ, Purdon TJ, van Leeuwen DG, Auid O, et al. Targeted delivery of a PD-1-blocking scFv by CAR-T cells enhances anti-tumor efficacy *in vivo*. Nat Biotechnol. 2018; 36: 847-56.
146. Knochelmann HM, Smith AS, Dwyer CJ, Wyatt MM, Mehrotra S, Paulos CM. CAR T Cells in Solid Tumors: Blueprints for Building Effective Therapies. Front Immunol. 2018; 9: 1740.
147. Martinez M, Moon EK. CAR T Cells for Solid Tumors: New Strategies for Finding, Infiltrating, and Surviving in the Tumor Microenvironment. Front Immunol. 2019; 10: 128.
148. Zhao Z, Xiao X, Saw PE, Wu W, Huang H, Chen J, et al. Chimeric antigen receptor T cells in solid tumors: a war against the tumor microenvironment. Sci China Life Sci. 2020; 63: 180-205.
149. Xie YJ, Dougan M, Jailkhani N, Ingram J, Fang T, Kummer L, et al. Nanobody-based CAR T cells that target the tumor microenvironment inhibit the growth of solid tumors in immunocompetent mice. Proc Natl Acad Sci U S A. 2019; 116: 7624-31.
150. Liu D, Zhao J, Song Y. Engineering switchable and programmable universal CARs for CAR T therapy. J Hematol Oncol. 2019; 12: 69.
151. Weiss T, Weller M, Guckenberger M, Sentman CL, Roth P. NKG2D-Based CAR T Cells and Radiotherapy Exert Synergistic Efficacy in Glioblastoma. Cancer Res. 2018; 78: 1031-43.
152. Minn I, Rowe SP, Pomper MG. Enhancing CAR T-cell therapy through cellular imaging and radiotherapy. Lancet Oncol. 2019; 20: e443-e51.
153. John LB, Devaud C, Duong CP, Yong CS, Beavis PA, Haynes NM, et al. Anti-PD-1 antibody therapy potently enhances the eradication of established tumors by gene-modified T cells. Clin Cancer Res. 2013; 19: 5636-46.
154. Serganova I, Moroz E, Cohen I, Moroz M, Mane M, Zurita J, et al. Enhancement of PSMA-Directed CAR Adoptive Immunotherapy by PD-1/PD-L1 Blockade. Mol Ther Oncolytics. 2017; 4: 41-54.